ADF300329

AD

AD-A133 756

MEMORANDUM REPORT ARBRL-MR-03306

DRIFT VELOCITY COMPUTATIONS FOR SHAPED-CHARGE JETS

Steven B. Segletes

DTIC
ELECTE
OCT 17 1983
A

September 1983

US ARMY ARMAMENT RESEARCH AND DEVELOPMENT COMMAND
BALLISTIC RESEARCH LABORATORY
ABERDEEN PROVING GROUND, MARYLAND

Approved for public release; distribution unlimited.

DTIC FILE COPY

83 10 17 008

**Destroy this report when it is no longer needed.
Do not return it to the originator.**

Additional copies of this report may be obtained from the National Technical Information Service, U. S. Department of Commerce, Springfield, Virginia 22161.

The findings in this report are not to be construed as an official Department of the Army position, unless so designated by other authorized documents.

The use of trade names or manufacturers' names in this report does not constitute indorsement of any commercial product.

UNCLASSIFIED

SECURITY CLASSIFICATION OF THIS PAGE (When Data Entered)

REPORT DOCUMENTATION PAGE

READ INSTRUCTIONS BEFORE COMPLETING FORM

1. REPORT NUMBER
MEMORANDUM REPORT ARBRL-MR-03306

2. GOVT ACCESSION NO.
AD-A133756

3. RECIPIENT'S CATALOG NUMBER

4. TITLE (and Subtitle)
DRIFT VELOCITY COMPUTATIONS FOR SHAPED-CHARGE JETS

5. TYPE OF REPORT & PERIOD COVERED

6. PERFORMING ORG. REPORT NUMBER

7. AUTHOR(s)
S. B. Segletes

8. CONTRACT OR GRANT NUMBER(s)

9. PERFORMING ORGANIZATION NAME AND ADDRESS
US Army Ballistic Research Laboratory
ATTN: DRDAR-BLT
Aberdeen Proving Ground, MD 21005

10. PROGRAM ELEMENT, PROJECT, TASK AREA & WORK UNIT NUMBERS
1L162618AH80

11. CONTROLLING OFFICE NAME AND ADDRESS
US Army Armament Research & Development Command
US Army Ballistic Research Laboratory (DRDAR-BLA-S)
Aberdeen Proving Ground, MD 21005

12. REPORT DATE
September 1983

13. NUMBER OF PAGES
81

14. MONITORING AGENCY NAME & ADDRESS (if different from Controlling Office)

15. SECURITY CLASS. (of this report)
Unclassified

15a. DECLASSIFICATION/DOWNGRADING SCHEDULE

16. DISTRIBUTION STATEMENT (of this Report)
Approved for public release; distribution unlimited.

17. DISTRIBUTION STATEMENT (of the abstract entered in Block 20, if different from Report)

18. SUPPLEMENTARY NOTES

19. KEY WORDS (Continue on reverse side if necessary and identify by block number)
shaped-charge jet
penetration
drift velocity
transverse velocity
drift distribution
sidewall impact

20. ABSTRACT (Continue on reverse side if necessary and identify by block number) bet/

This work provides quantitative support for the assumption that jet curvature is the major cause for nonideal jet penetration. Jet radiographs were analyzed to ascertain the component of jet velocity normal to the axis of symmetry of the charge for each jet particle. This nonideal velocity component is the drift velocity. The drift velocity distribution determined in this manner was imposed on the jet in a computer simulation of the penetration process. The computer code, referred to as PENJET, was employed to generate penetration-standoff

DD FORM 1 JAN 73 1473 EDITION OF 1 NOV 65 IS OBSOLETE

UNCLASSIFIED

SECURITY CLASSIFICATION OF THIS PAGE (When Data Entered) curves using the data from a specific round. This curve depicts the penetration-standoff performance for the single round as if it could be shot repeatedly at a variety of standoffs. The curve could then be compared with the actual datum for the round.

TABLE OF CONTENTS

DTIC COPY INSPECTED 2

LIST OF ILLUSTRATIONS

PRECEDING PAGE BLANK-NOT FILMED

LIST OF ILLUSTRATIONS (CONT'D)

I. INTRODUCTION

Theories to predict penetration of shaped charges have met with varying degrees of success. Except for relatively short standoffs, penetrations diverge greatly and never really approach idealized values. Inspection of jets through the use of flash radiographs reveals why idealized penetration is not a reality: because the idealized jet is not a reality. The presence of drift velocity (seen in a radiograph as jet curvature) is suggested as being the main cause for the variance in jet penetrations. Transverse (or alternately drift) velocity refers to the motion of shaped-charge jet particles in the plane perpendicular to the charge axis of the warhead (drift or transverse plane). The distance travelled by a jet particle in the transverse plane is referred to as the particle deviance.

All shaped charge jets contain drift velocity to some degree or another. The origins of drift are naturally linked to imperfections in the warhead itself. Lack of uniformity of liner thickness, nonhomogeneous explosive, as well as asymmetric liner confinements must all be considered as possible causes of drift velocity in any given round. Fissures in the explosive material and uncentered boosters can also contribute to jet performance that is less than perfect. With respect to the rounds studied in this analysis, it was also noticed that rounds with pressed explosive possessed consistently lower penetration capabilities than their cast explosive counterparts. One theory is that the high pressures (20,000 psi) required to press the explosive were capable of distorting the liner. The problems characterizing these pressed rounds were typical of the early days of pressing. Technology in the area of pressing explosives has since improved to a point where many of the problems then inherent in the rounds studied have been corrected. Some uncased pressed rounds now show penetrations of 5.5 calibers at 24 caliber standoff. Nonetheless, the pressed rounds that were studied possessed adverse qualities that manifested themselves in poor jets. Thus, with a multitude of sources for asymmetric conditions always present, it is not surprising to find the regularity with which drift velocity occurs in jets.

An algebraic analysis can be performed to evaluate numerically the drift velocities of the particles of a given jet. Preliminary and somewhat simplified computations indicate that drift velocity alone is sufficient to account for major variations in jet penetration.

II. MEASURING THE DRIFT VELOCITY OF A PARTICLE

The flash radiograph is the best tool to perform detailed analysis of the shaped charge jet in flight. It would, therefore, be appropriate to explain the nature and setup of the apparatus and how it relates to the data obtained and used in the analysis. A diagram of the apparatus is shown in Figure 1. The jet is radiographed from three different angles at three different times before it finally penetrates the target. The angular separation of each of the x-ray tubes is 45°. A sample radiograph of one of the rounds studied is shown in Figure 2. Note the fiducial markings which

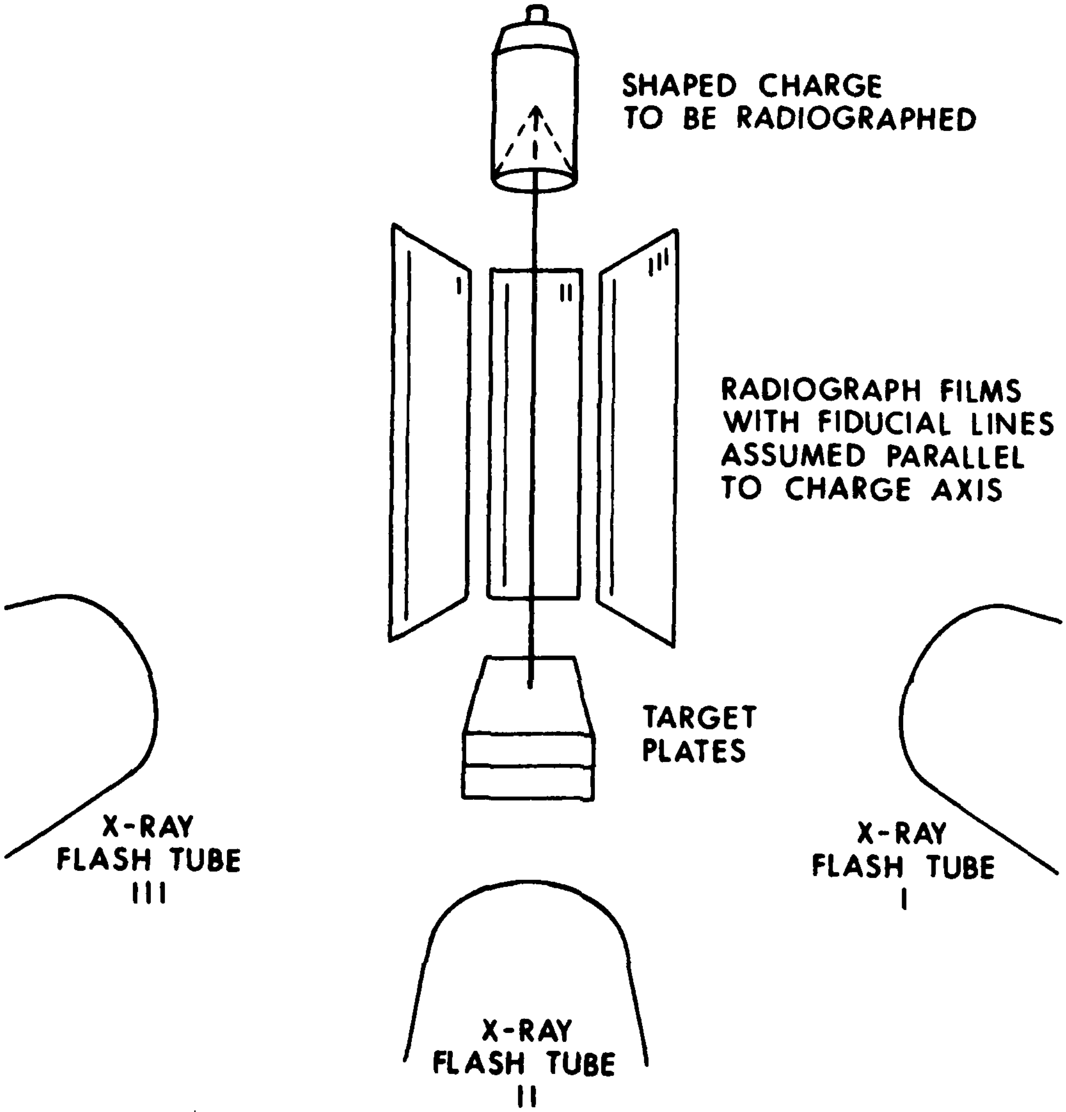

Figure 1. Radiographic Apparatus Used to Record Flight of Shaped-Charge Jet

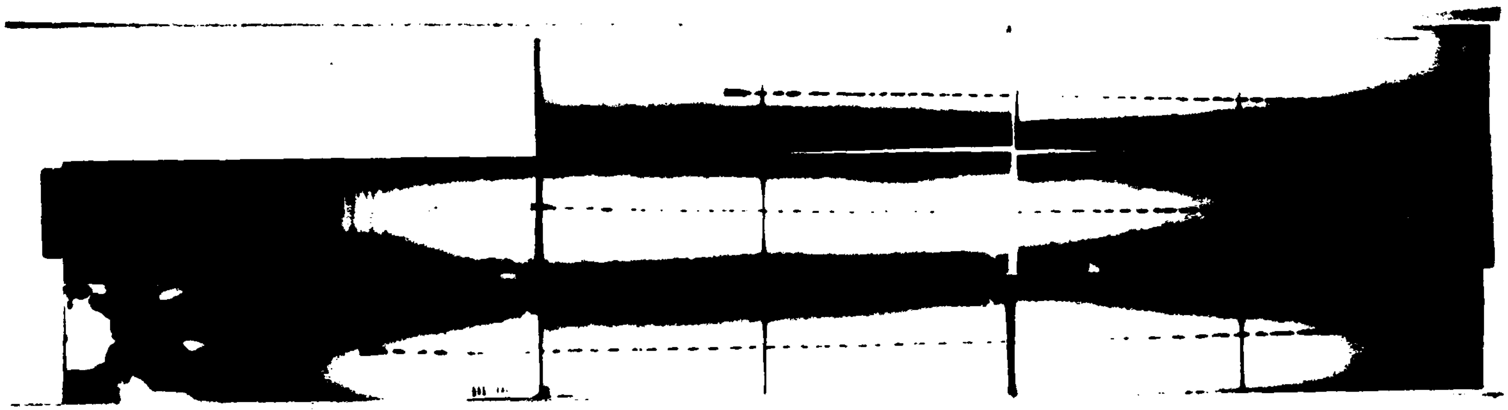

Figure 2. Sample Radiograph of a Shaped-Charge Jet in Flight

lie not on but parallel to the charge axis. Data are extracted from the radiographs by a digitizing process whereby each particle on the film is defined by six points located on the perimeter of the particle. By this means, calculations are made for each particle's length, diameter, velocity, mass, momentum, and kinetic energy using procedures described by Blische and Simmons.[1]

If it is assumed that the fiducials are parallel to the charge axis of a round, the radiograph of an ideal jet would contain an image of the jet parallel to the fiducials on all exposures. This assumption is not strictly true, but shall be discussed in Section IV. With near perfect jets rarely being observed, it becomes important to measure the transverse movement of particles with respect to the charge axis. However, the location of the charge axis is, in itself, unknown. One assumes that the charge axis is parallel to the fiducials on all radiograph exposures, though it is not coincident with any one of them. It becomes necessary, therefore, to choose a workable reference. The rear of the jet has always been considered the most stable portion. For this reason, a particle near the rear of the jet that is readily definable in all three radiographs is chosen as the reference. The reference axis is an axis parallel to the warhead charge axis on which the reference particle lies. If the reference particle is not drifting in the transverse plane, the reference axis will be coincident with the charge axis.

To see how the transverse velocity of a particle might be measured, it would be convenient to imagine looking down the charge axis, as if from liner to target. Ignoring all particles of the jet except the reference particle and the particle in question, the charge axis view of the situation could be described by Figure 3. Note that the film shown in the figure is just the "edge" of the film since the view is down the charge axis. The deviance (perpendicular distance between the reference axis and the particle in question) that is seen in the radiograph is less than or at most equal to the actual deviance due to the cosine effect. Given the apparatus of Figure 1, and having exposed the three radiographs simultaneously, the reference particle and the particle in question could be precisely located with respect to each other in the transverse or drift plane. This situation is illustrated in Figure 4. The time delay that actually exists among the three exposures complicates matters little and three governing equations are readily derived:

$$V_T^* = \frac{D_1/\cos(\theta+45°)}{t_1} \tag{1}$$

$$V_T^* = \frac{D_2/\cos\theta}{t_2} \tag{2}$$

[1] *J. Blische, B. Simmons, "A Method for Reducing Data from Radiographs of Shaped-Charge Jets," BRL Report ARBRL-TR-02330, Jun 81 (AD A102770).*

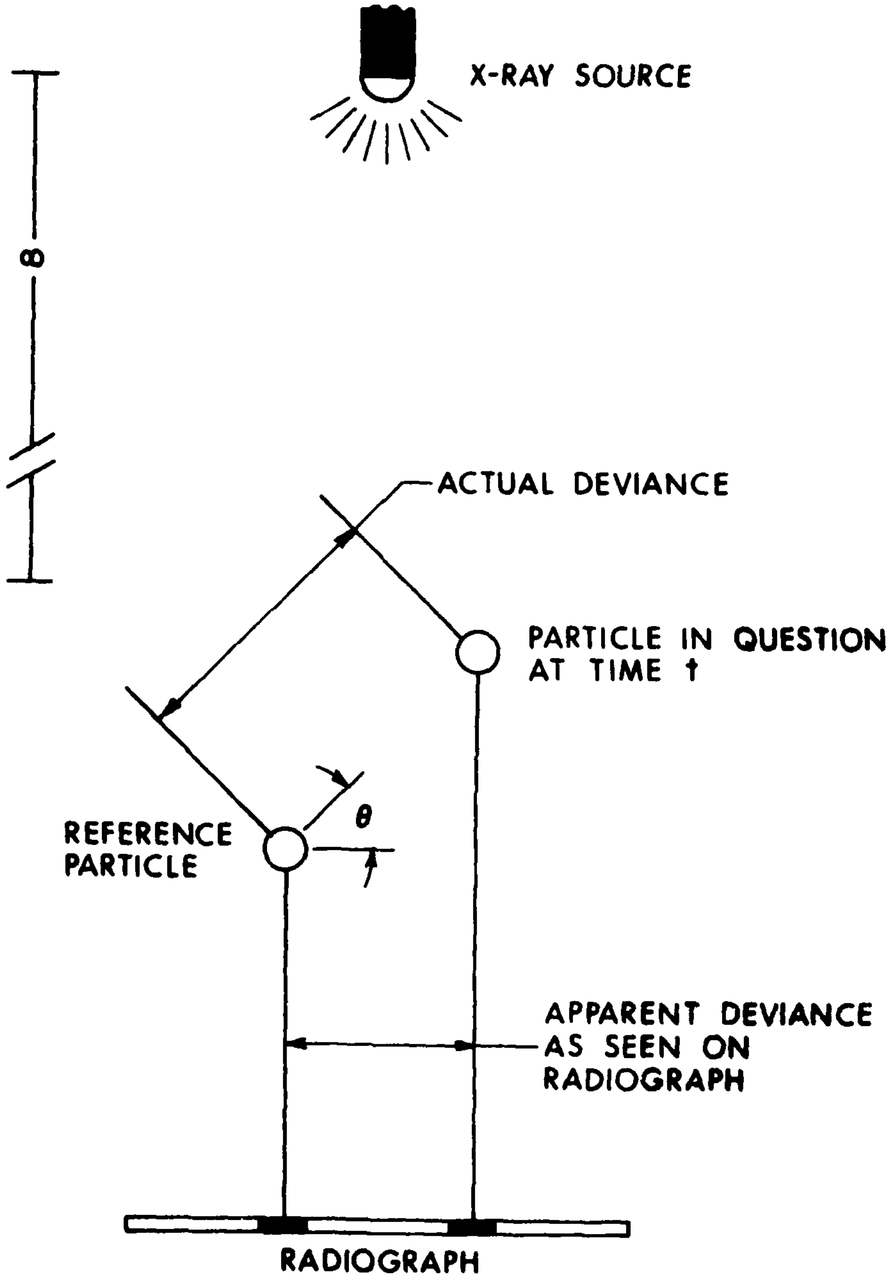

Figure 3. View of Particle Deviation as Projected onto the Transverse Plane

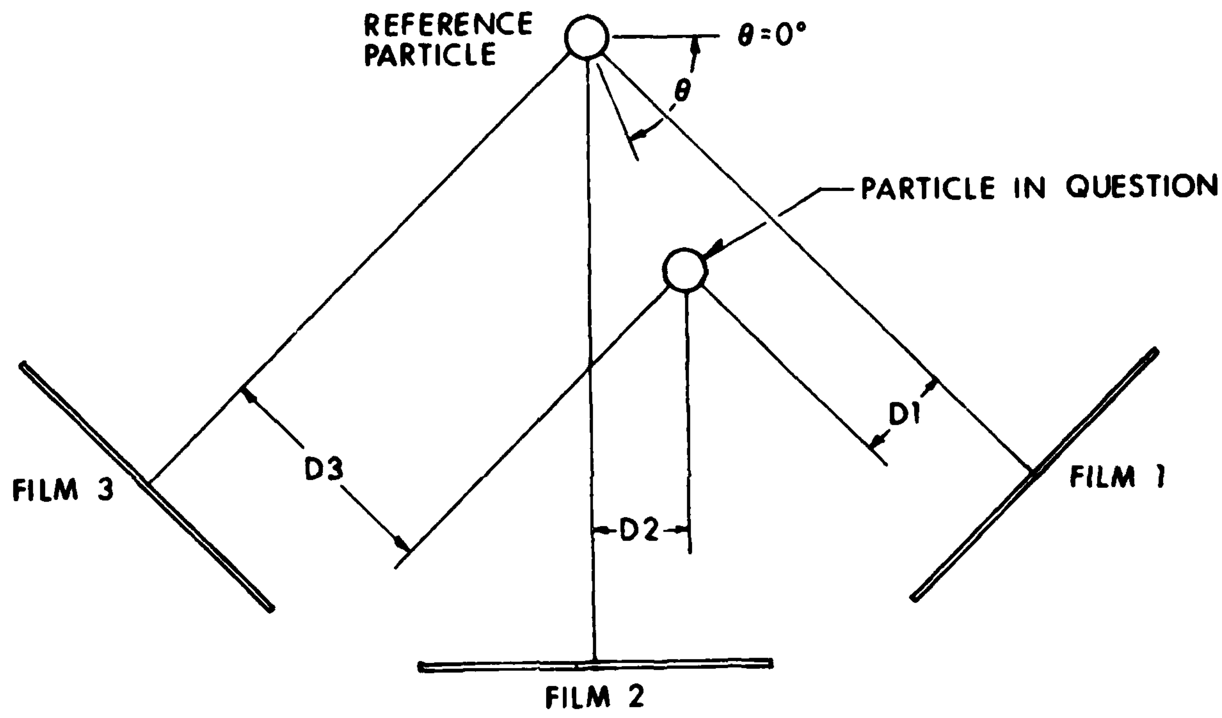

Figure 4. Locating a Particle in the Transverse Plane Through the Use of Three Radiographs

$$V_T^* = \frac{D_3/\cos(\theta-45°)}{t_3} \qquad (3)$$

where D_k - apparent deviance read off the K'th radiograph

t_k - the time between particle formation and the K'th exposure

θ - deviation angle between path of deviation and some arbitrary reference (chosen parallel to film 2)

Equations (1), (2), and (3) all contain two unknowns, namely magnitude of drift velocity (V_T^*) and angle of deviation (θ). Any two of these three equations can be solved simultaneously to yield a result for transverse velocity, both in magnitude and direction. In reality, the equations are solved in all three combinations, and a weighted average is taken depending on the particle's orientation with the radiographs. This velocity shall be called by the name of relative drift velocity since the particles are moving with respect to a moving reference (the reference particle).

III. THE DRIFT VELOCITY DISTRIBUTION FOR A GIVEN ROUND

When relative transverse velocities are evaluated for all the particles of a jet, a polar plot can be made whereby a line segment with length proportional to the magnitude of drift velocity is plotted at the appropriate deviation angle in the transverse plane. A sample velocity fan is shown in Figure 5. This relative velocity fan shows a kind of spray of the jet particles away from the reference particle in the deviation plane.

When a plot is made of the axial versus transverse particle velocity for a given round, a graph similar to Figure 6 frequently results. The data seems to be of the form:

$$V_A = KV_T^* + V_{REF} \qquad (4)$$

where: V_A - axial velocity of particle

V_T^* - relative transverse velocity of particle

K - constant varying from round to round

V_{REF} - axial velocity of the reference particle

Most rounds studied were in high correlation with Equation (4).

The next quantity to determine is the drift velocity of the reference particle from which all the calculations were made. If we assume that the reference drift velocity is negligible, then the separation distance between impacts of the jet tip and the reference particle would routinely exceed

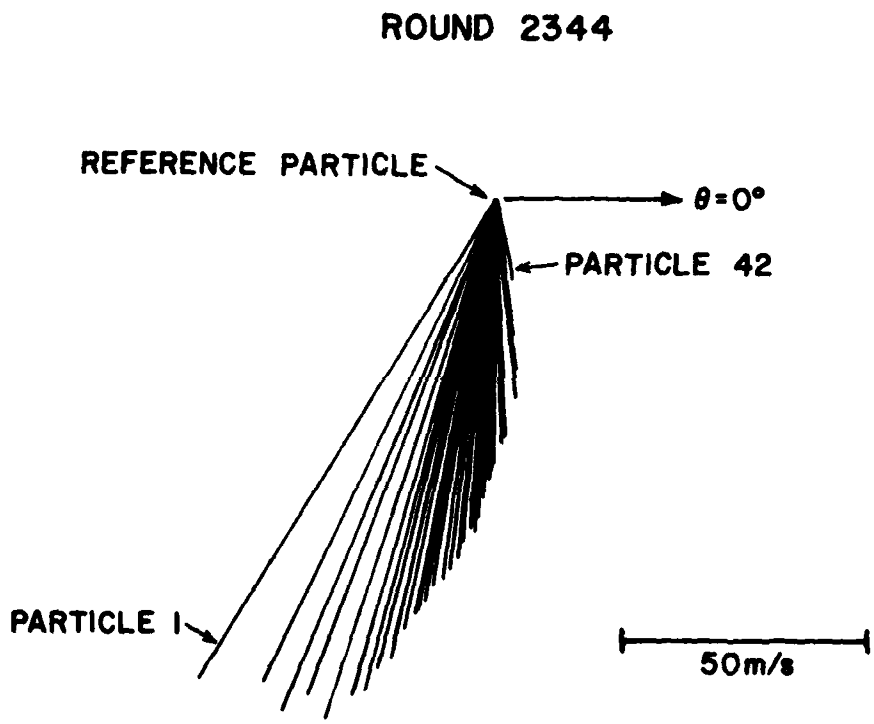

Figure 5. Relative Velocity Fan Showing the Pattern Formed by the Drifting Jet Particles

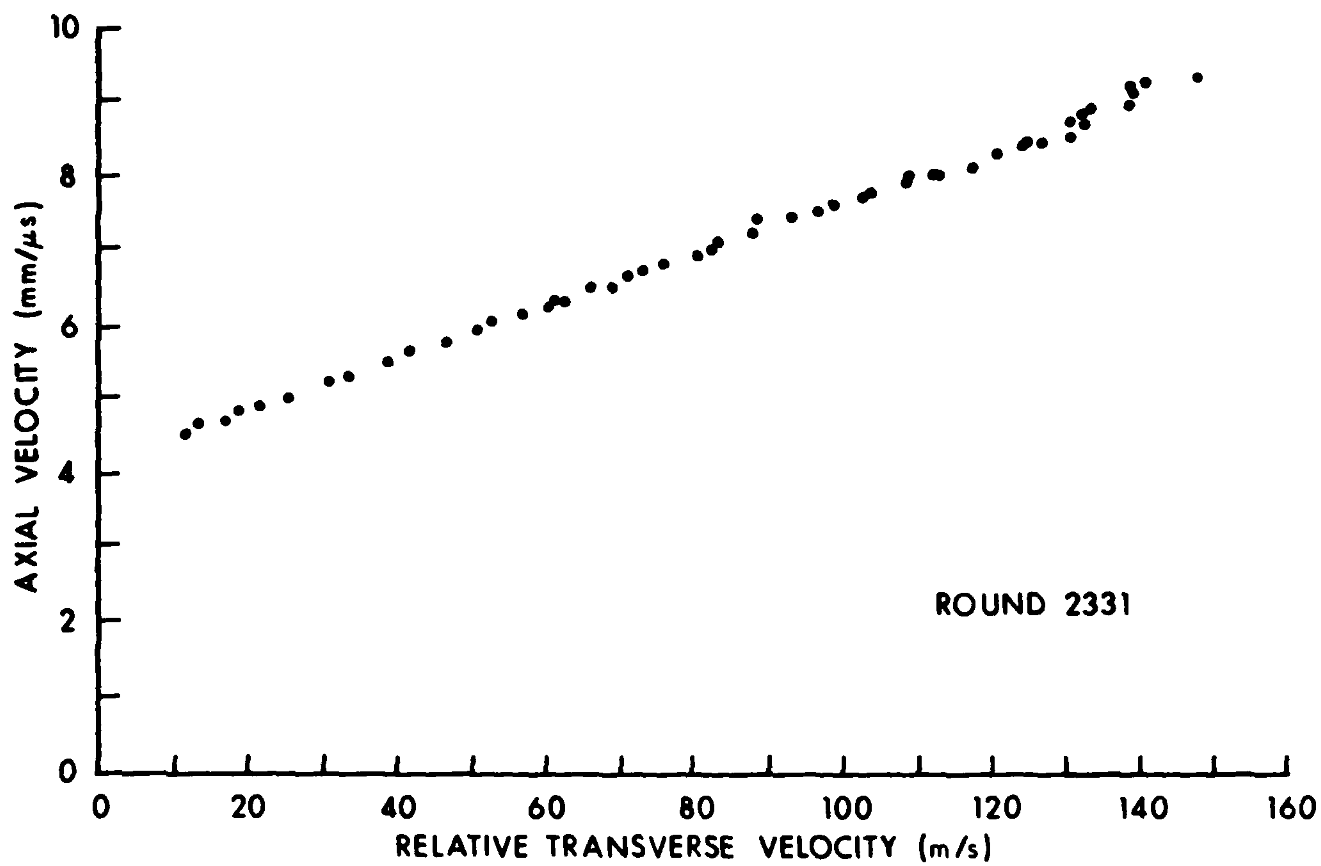

Figure 6. Typical Plot of Axial vs. Transverse Velocity for Particles of a Given Round

1/2 charge diameter (CD) at a 24 CD standoff for typical drift distributions studied. Under such conditions, the reference particle will never enter the crater created by the jet tip because of excessive drift. However, it is not uncommon for a jet to produce a single entrance hole into the target at 24 CD standoff. Thus, the reference must possess a drift velocity which will tend to bring the reference into the crater formed by the jet tip. An equation is needed which expresses that the reference particle should deviate the same distance from the charge axis as the jet tip upon reaching a target block at a given standoff. Mathematically, the assumption is:

$$D_R = D_j \tag{5}$$

where: D_R - the distance the reference has deviated upon reaching the target surface (magnitude only)

D_j - the distance the jet tip has deviated upon reaching the target surface (magnitude only)

Equation (5) does not preclude drift among the jet particles since it pertains to magnitude only. An angular separation of the drifting particles still exists and will tend to separate the jet particles at extended standoff. For a small angular deviation among jet particles however, Equation (5) gives jets the ability to produce single crater target impacts. It is suggested solely because a compensatory reference particle drift was required and is the best which can be proposed at this time. Since drift velocity is assumed to be constant after a particle's formation, Equation (5) can be expressed as:

$$V_{T_R} t_R = V_{T_j} t_j \tag{6}$$

where: V_T - the absolute drift velocity of the associated particle

t - the time required for the associated particle to reach the target surface

R - the reference particle

j - an arbitrary jet particle

But the time required for a particle to reach the target surface is equal to the standoff as measured from the virtual origin (Z_o) divided by the particle's axial velocity (V_A). Therefore, Equation (6) expands to:

$$V_{T_R} \frac{Z_o}{V_{A_R}} = V_{T_j} \frac{Z_o}{V_{A_j}} \tag{7}$$

Simplifying:

$$\frac{V_{A_R}}{V_{T_R}} = \frac{V_{A_j}}{V_{T_j}} \tag{8}$$

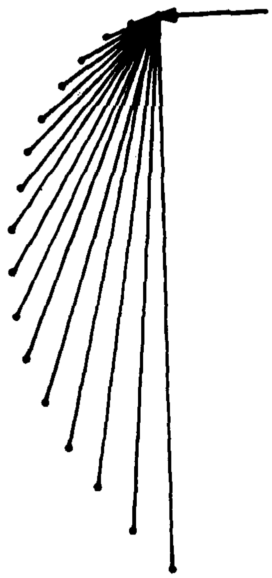

A RELATIVE VELOCITY FAN WITH SCALED REFERENCE VELOCITY ARROW INDICATING MAGNITUDE AND DIRECTION OF REFERENCE DRIFT. THE APEX OF THE FAN REPRESENTS THE REFERENCE PARTICLE FROM WHICH DRIFT MEASUREMENTS WERE ORIGINALLY TAKEN.

AN ABSOLUTE VELOCITY FAN IS CREATED BY CONNECTING THE TAIL OF THE REFERENCE VECTOR TO THE RELATIVE VELOCITY FAN. THE APEX OF THE FAN LOCATES THE CHARGE AXIS IN THE TRANSVERSE PLANE. THE REFERENCE PARTICLE NOW BECOMES JUST ANOTHER DRIFTING PARTICLE.

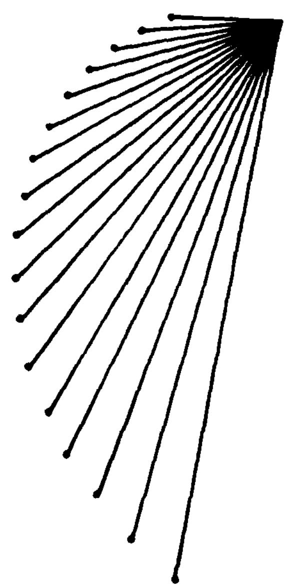

Figure 7. Transformation of Relative Fan Into Absolute Fan for a Hypothetical Drift Distribution

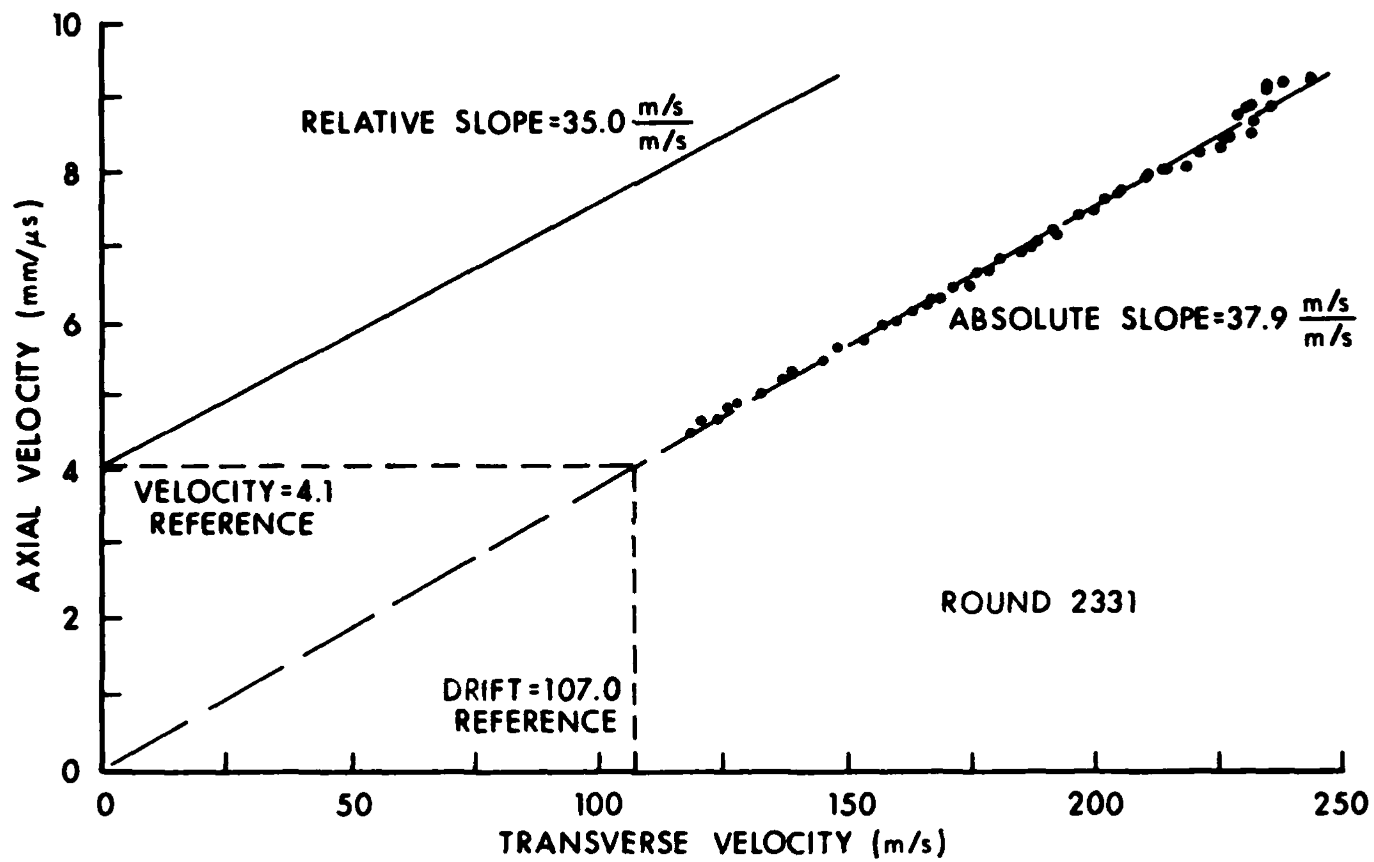

Figure 8. Effect of Transformation from Relative to Absolute Drift Velocity on the Slope of the Curve

For a crater profile in which all particles of the jet enter the target surface at the same point, Equation (5) must hold for all particles, implying:

$$\frac{V_A}{V_T} = \text{constant} \tag{9}$$

Since the reference is at the apex of the relative transverse velocity fan, the reference velocity would appear as a vector with its tip attached to the apex of the relative velocity fan. Its length corresponds to the drift velocity of the reference particle and its direction indicates the direction in which the reference is deviated. Its direction of deviation is assumed to be about the same as that of the slowest digitized particle. The absolute velocities of the balance of the particles are calculated by vectorially adding the reference velocity to the relative velocities of the respective particles. Thus, an absolute drift velocity fan is created by drawing the segments from the tail of the reference vector to the tips of the relative drift velocity fan. (See Figure 7.) Graphically, Equation 9 implies a linear V_A vs. V_T plot which intercepts the origin. With the proper vectorial addition of the reference drift as just described, relative drift distributions like Figure 6 readily map into absolute drift distributions which satisfy Equation 9. (See Figure 8.)

There is no way to know whether this transformation into absolute velocities is the correct one. However, it is believed that the directional assumption of the reference is a safe one, and that the Equation (5) assumption is as good as any considering the need for the drift correction of particles. In addition, the results obtained from the transformation are supported by the experimental data. Note that Equation (9) does not guarantee that all particles will only form a one-crater hole profile even though all the particles should deviate the same distance from the charge axis. A large angular spread in a jet (characterized by a wide absolute velocity fan) may produce enough relative deviation among the particles so as to cause multiple impacts at long standoff. Thus, the deviating factors in jets are both the angular spread and the magnitudes of the drift velocities.

IV. THE QUESTION OF TILT

A possible and potentially fatal flaw in the previous discussion concerns the presence of tilt. The word tilt is taken to mean a charge axis that is not parallel to the radiograph fiducials. An original assumption was that there was no tilt, or that charge axis and fiducials were aligned. It is obvious that some sort of tilt must exist, however small. The answer as to when tilt becomes critical is a bit disconcerting. Depending on the jet, a one-degree tilt of the charge axis off the fiducials could induce an apparent drift velocity of 160 m/sec in the jet tip as measured with respect to the fiducials. It is likely that uncertainties of this magnitude exist regularly.

The consequence of tilt on a jet is an apparent drift velocity distribution, which is also governed by Equation (9), which is the assumed relation for actual drift velocity. One may rightfully wonder whether all of the drift velocities read off the radiographs are due completely to tilt, and whether graphs like that of Figure 6 are a consequence of tilt alone. In fact, what is read off the radiographs is the superposition of both tilt and real drift velocity distributions. However, it should be noted that an important aspect of tilt is that it cannot produce a velocity fan. All of the particles of a jet under the influence of tilt exclusively would appear to drift in a uniform direction. Yet, Equation (9) has been seen to hold for jets with velocity fans spanning in excess of 90°.

The concern here is whether a nonlinear drift distribution could be "tilted" into appearing linear on the radiographs, and thus explain the data without having the actual drift obey Equation (9). Such could only be the case if the magnitude of actual drift were small in relation to tilted drift. If this were the case, however, the angular spans of the velocity distributions would also be quite small, which is usually not the case. Thus, it appears that the actual drift velocities are at least of the same order of magnitude as the apparent drift velocities due to tilt. Thus, it seems that the actual drift distributions, though probably different from the measured drift distributions, can still be adequately described by Equation (9). This belief is based only on the rounds studied. No explanation is offered as to why there might be a relation between the axial and transverse velocities of jet particles. Also, it is uncertain as to whether this may be a general phenomena or characteristic only of the rounds studied.

Support for Equation (9) was found in work done by Aerojet General Corporation.[2] Aerojet was interested in the crater formation of individually impacting particles. A shaped charge supplied the particles for their experiment. The method employed for dispersion of the particles was asymmetric initiation. Considering that it was desired to induce much drift velocity in the particles, the effects of tilt could be neglected in this experiment. The target plate used in their experiment is shown in Figure 9. The particle impacts generally lie at a constant distance from the slug impact. Assuming the slug flight path to be coincident with the charge axis, Equation 9 is the governing equation.

A penetration code was created to predict penetrations for nonideal shaped-charge jets. Unlike the DSM model,[3] which can express penetration in a single equation, the model developed analyzes the jet piecemeal. It is described in detail in the following section.

---

[2] K. N. Kreyenhagen, J. E. Ferguson, R. R. Randall, J. P. Joyce, "Special Explosive Projectors," Proc. 6th Symposium Hypervelocity Impact, Vol. I (Held Cleveland, Ohio, April 30-May 2, 1963).

[3] R. DiPersio, J. Simon, A. Merendino, "Penetration of Shaped-Charge Jets Into Metallic Targets," Ballistic Research Laboratory Report No. 1296, September, 1965 (AD 476717).

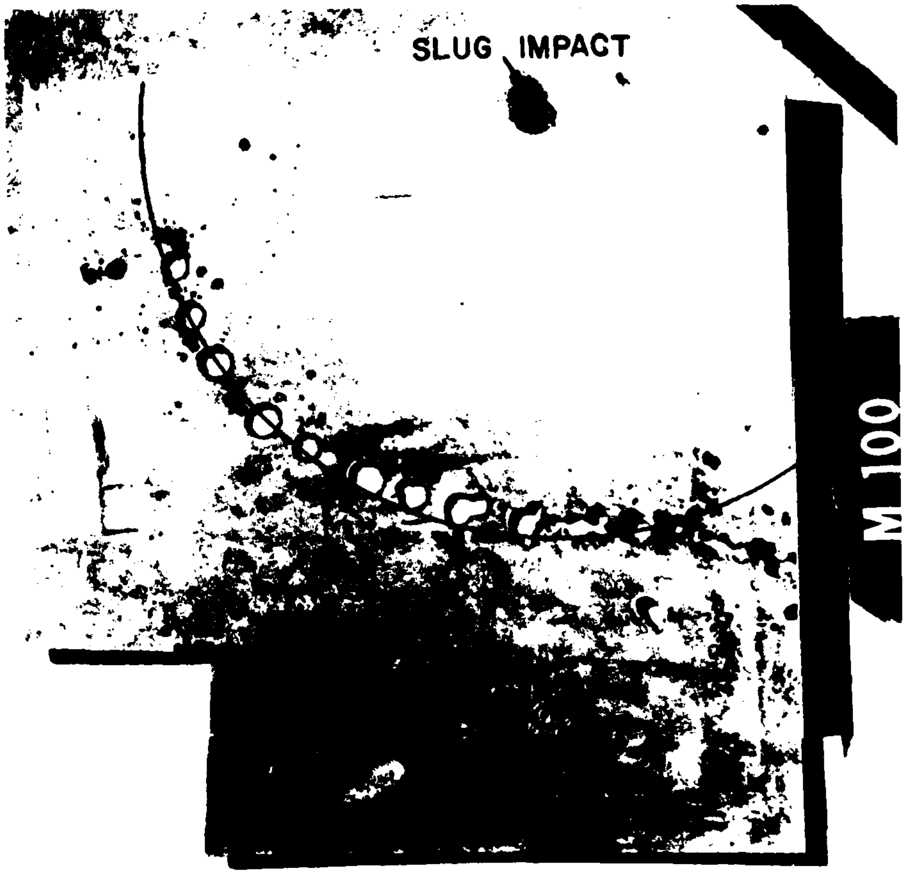

Figure 9. Target Plate for Asymmetrically Initiated Shaped Charge (Reference 2)

V. THE CREATION OF A PENETRATION CODE TO ANALYZE DRIFT

The purpose of analyzing drift velocity distributions of shaped-charge jets is to see how these distributions affect penetration. The dynamics of penetration is not, however, a thoroughly understood subject. Many theories exist in attempts to discribe the mechanical properties of matter. Classical, empirical and even wave mechanical concepts are used in pursuit of the subject. Consequently, rather than adding to the spectrum of theories that already exist, the author chose to draw upon information already available on the subject whenever possible and to combine views in a seemingly compatible manner.

One shaped-charge penetration model that has received much attention in recent years was formulated by DiPersio, Simon, and Merendino (the DSM model).[3] This model does a good job at predicting penetration of shaped charges even at extended standoffs. The model accomplished this however, by implying that there exists a cutoff penetration velocity, a minimum penetration velocity below which a jet cannot penetrate. Unfortunately, the DSM cutoff penetration velocity implies that jet material traveling below certain hypervelocity speeds is incapable of penetrating target material. Substantial quantities of jet material are thus eliminated from the penetration process. The DSM model is empirically based and really attempts only to describe the data at hand and does not enter an intense theoretical discussion to describe the origins of jet cutoff other than citing that it exists experimentally. The work presented in this report suggests that the drift of particles off axis is largely responsible for reduced jet penetration, whereby drifting particles strike the target not at the bottom of the hole but somewhere up the hole profile. This commencement of sidewall impacts frequently seems to constitute a cutoff in jet penetration, since the overall depth of penetration is not altered by a sidewall impact.

A method, therefore, had to be devised which would allow penetration to be a function of drift velocity. Three-dimensional finite difference codes were not considered due to a coupling of availability and cost. Yet, a three-dimensional description of penetration was required since the source of altered penetration is the spread of the particles off of the one-dimensional axis. Consequently, all aspects of particle penetration would have to be considered: size, shape, and orientation of crater formation in a three-dimensional target block.

The code developed in the present work (referred to as PENJET) includes many simplifications and assumptions. The first assumption concerns the shape of crater formed by an impinging jet particle. The chosen shape was that of an ellipsoid, with the ellipsoid being characterized by a position in three-dimensional space, dimensions along the axes, as well as an orientation in space (as shown in Figure 10). The position of particle impact is determined by using the velocity fan of a round to trace the particles' flight through three-dimensional space and time in order to locate the particle position with respect to the instantaneous hole profile (formed by earlier particles of the jet). If a particle is found to strike any point within the target, PENJET then proceeds through a series of calculations to determine the remainder of crater parameters. Once the crater formed by a particle is effectively evaluated, PENJET proceeds through subsequent particles of the jet until impacts for all digitized particles have been evaluated. Thus,

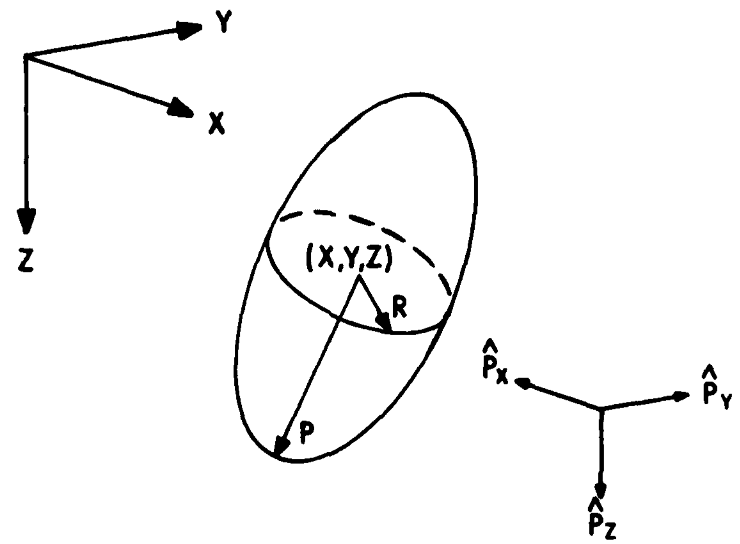

(X,Y,Z)	LOCATION OF IMPACT IN 3-D SPACE
P	MAGNITUDE OF PARTICLE PENETRATION
R	MAGNITUDE OF CRATER RADIUS
$\hat{P}_X, \hat{P}_Y, \hat{P}_Z$	PENETRATION AXIS (A UNIT VECTOR IN 3-D SPACE)

Figure 10. Parameters Generated by PENJET to Describe Crater Formed by Impinging Jet Particle

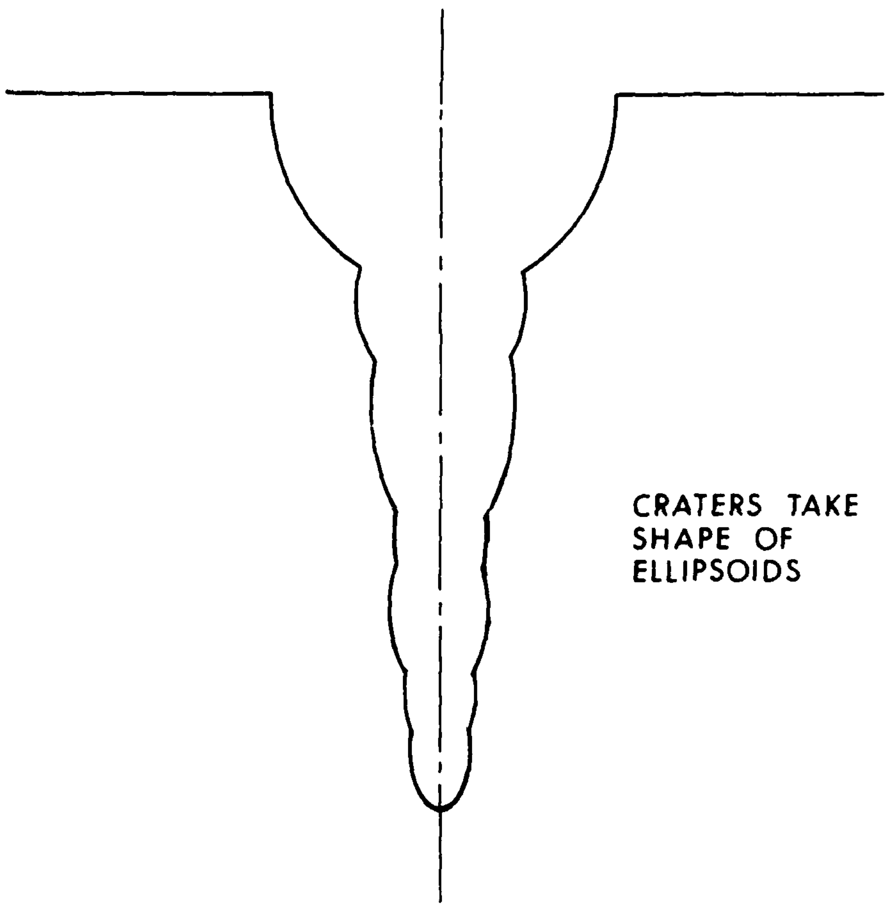

Figure 11. PENJET Hole Profile Results from Ellipsoid Superposition

a hole profile for a complete jet is just the superposition of ellipsoids from each of the particle impacts. A two-dimensional representation of a three-dimensional hole profile is shown in Figure 11 for a fictitious nondrifting jet. When evaluating the crater formed by an impinging jet particle, crater volume is a constraining factor. That is to say, crater volume is calculated independently of other crater parameters and is assumed to be a function of particle kinetic energy alone. Subsequent calculations for actual crater dimensions are, therefore, constrained by the allowable volumetric target displacement a given particle can produce. The function governing the volume energy relationship is a linear one, similar to that adopted by DiPersio, Simon, and Merendino.[3] The distinction arises in the fact that the DSM model expresses its proportionality constant as a relationship between total jet kinetic energy and total hole volume. PENJET, on the other hand, bases its constant on the energy of the individual particle. It is not surprising to find, therefore, that the DSM constant differs from its PENJET counterpart. Consider also, that the energy constant of PENJET does not strictly define an exact amount of displaced target material. As mentioned previously, the hole profile of PENJET is the superposition of ellipsoid craters corresponding to each of the jet particles. The orientation of these ellipsoids will greatly affect the spacial overlap of the ellipsoids, and thus the overall volumetric target displacement of a given jet. Because of this spacial overlap of particle craters, the overall crater volume as calculated by PENJET is not the summation of particle energies divided by the energy constant. Estimation of the constant was gotten empirically through examination of target blocks as well as hole profile data.

The crater shape of an individual impact is prescribed (as an ellipsoid) and the particle's crater volume is proportional to its own kinetic energy. Therefore, knowledge of a particle's penetration capability will allow the particle's hole radius to be computed and vice versa. In PENJET, depth of penetration is computed, with crater radius being subsequently determined. The model of particle penetration used in the code is based on the work of Fitzgerald,[4] who draws on the work of Kineke[5] to imply that crater formation occurs in a direction perpendicular to the stricken surface. Fitzgerald calls this phenomenon the wave refraction theory and shows that it applied to a single particle striking a flat plate at some obliquity (Figure 12). PENJET uses the concept in a more general sense by applying the wave refraction theory to local obliquities as well. Local obliquity is defined as the angle between the particle flight axis and the normal to the impact plane. Unless the impinging particle strikes exactly at the bottom of the hole profile, the refracted penetration wave will not be normal to the original target surface (Figure 13). In the strict sense, the refracted wave theory should only be applicable in the regime of hydrodynamic penetration. A large majority of particle impacts studied did not fit the qualification for hydrodynamic penetration. For these cases, the direction of penetration would be somewhere between the particle flight axis and the refracted wave axis. It was later noted that the penetration of a particle typically varied less than 5% because of the refracted wave assumption.

[4]*E. Fitzgerald, Particle Waves and Deformation in Crystalline Solids, Interscience Publishers, New York, 1966.*

[5]*J. Kineke, Jr. "An Experimental Study of Crater Formation in Metallic Targets," Proc. 4th Symposium Hypervelocity Impact, Vol. I (Held Eglin AFB, Florida, April 26-28, 1960).*

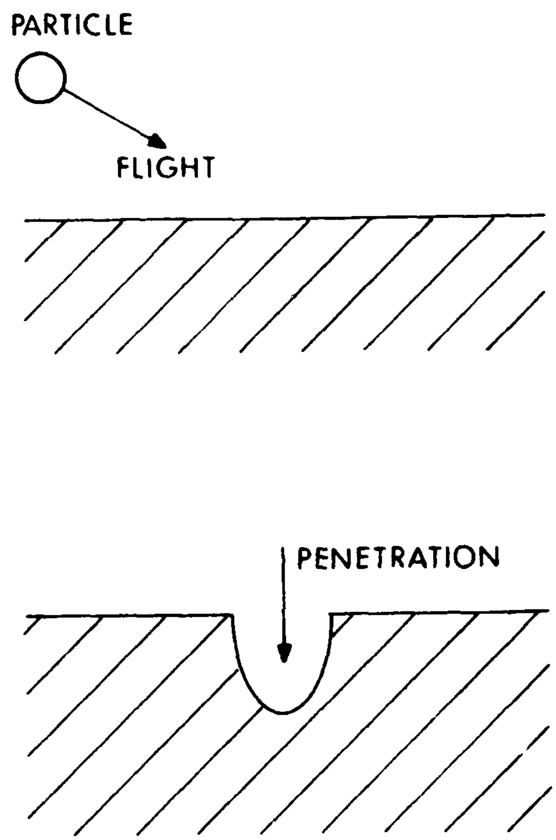

Figure 12. Crater Formation According to Refracted Particle Wave Theory

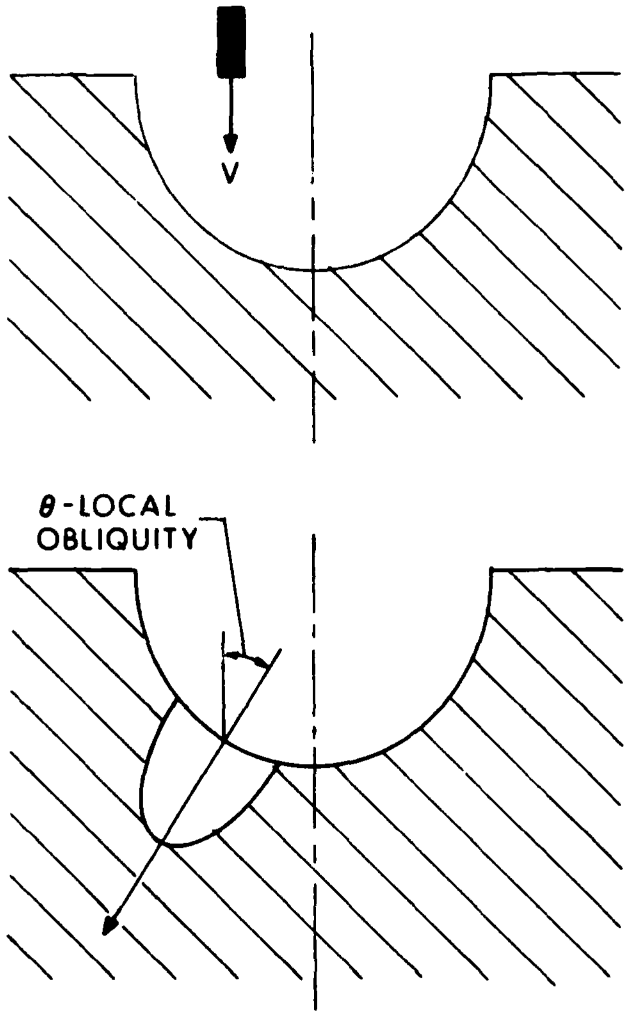

Figure 13. Refracted Particle Wave Theory Applied to Local Obliquity

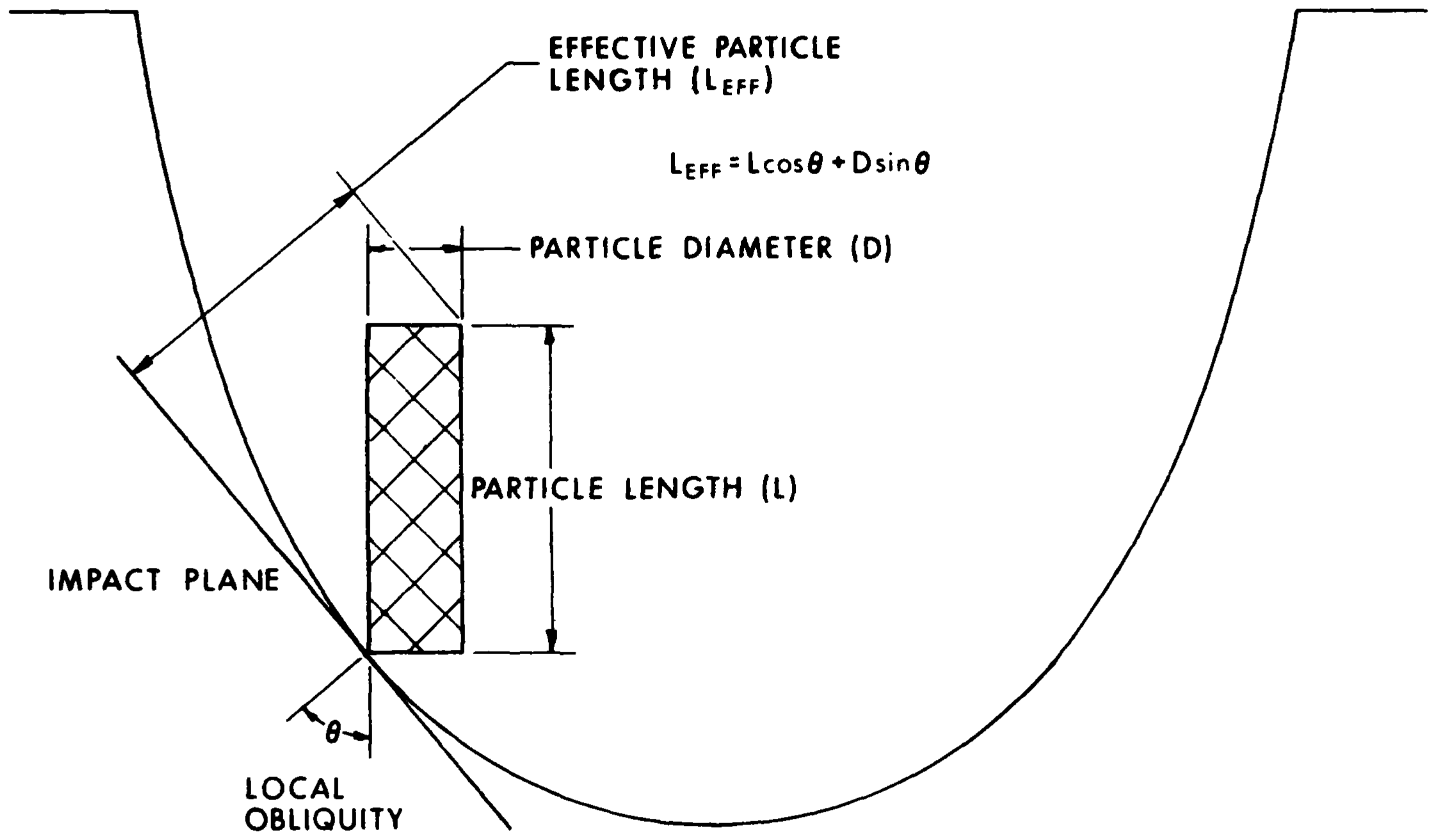

Figure 14. Concept of Effective Length as Seen by Impact Plane

Jet penetration in the continuous mode is quite a different matter from in the particulate mode. Modifications, therefore, had to be included to describe continuous jet penetration. The criterion on which to base mode of penetration is that of breakup time. PENJET uses a linear breakup equation whereby the jet tip particulates at some t_{min} and subsequent particle breakup occurs at regular Δt intervals. Estimates of jet particulation are obtained through examination of the radiographs for the three different exposures. These estimates are then used in a least squares fit to evaluate t_{min} and Δt. Based on the estimated breakup time, it can be established whether a given particle will be penetrating continuously or particulately at a given standoff. If continuous, the length of the particle is re-evaluated such that:

$$\ell_{CONTINUOUS} = \frac{t_{IMPACT}}{t_{BREAK}} \ell_{PARTICULATED} \tag{10}$$

Also, it is assumed that jet penetrating in the continuous mode does not experience the refracted particle wave of Figure 12. This must, of course, be the case since the continuous particle is essentially beginning its penetration exactly when and where the previous particle leaves off.

PENJET also considers particle orientation with respect to the stricken crater surface. The assumed shape of a shaped-charge particle is cylindrical, being characterized by a length and diameter. As local obliquity is increased, the length of the particle as seen by the impact point is effectively changed. (See Figure 14.) The extreme case is when local obliquity approaches 90°. In this case, the effective length of the particle approaches the diameter of the particle. Hydrodynamically, the penetration of a particle is proportional to the particle length. Thus, the effective particle length replaces the particle length in penetration calculations.

The presence of obliquity raises more questions. The larger the obliquity, the smaller the component of particle velocity perpendicular to the stricken surface. Once in the hypervelocity regime, large changes in particle velocity produce relatively small changes in penetration. If particle velocity is too small, however, the strength of the target and jet play a major role in reducing the penetration of that particle. Besides the effective particle length that the target "sees", it is believed that an effective velocity also plays a role in determining depth of penetration. Whereas penetration is assumed to be directly proportional to effective length, the role that effective velocity plays is not nearly so profound. As long as the effective velocity is in the hypervelocity regime (arbitrarily chosen as any velocity above 2mm/μsec), penetration is assumed greater than the effective particle length for copper jet into an RHA target. As effective velocity increases, penetration is assumed to asymptotically approach the hydrodynamically idealized value. That is:

$$\Delta P \rightarrow L_{eff}/\gamma \text{ where } \gamma = \sqrt{\rho_T/\rho_j} \quad .$$

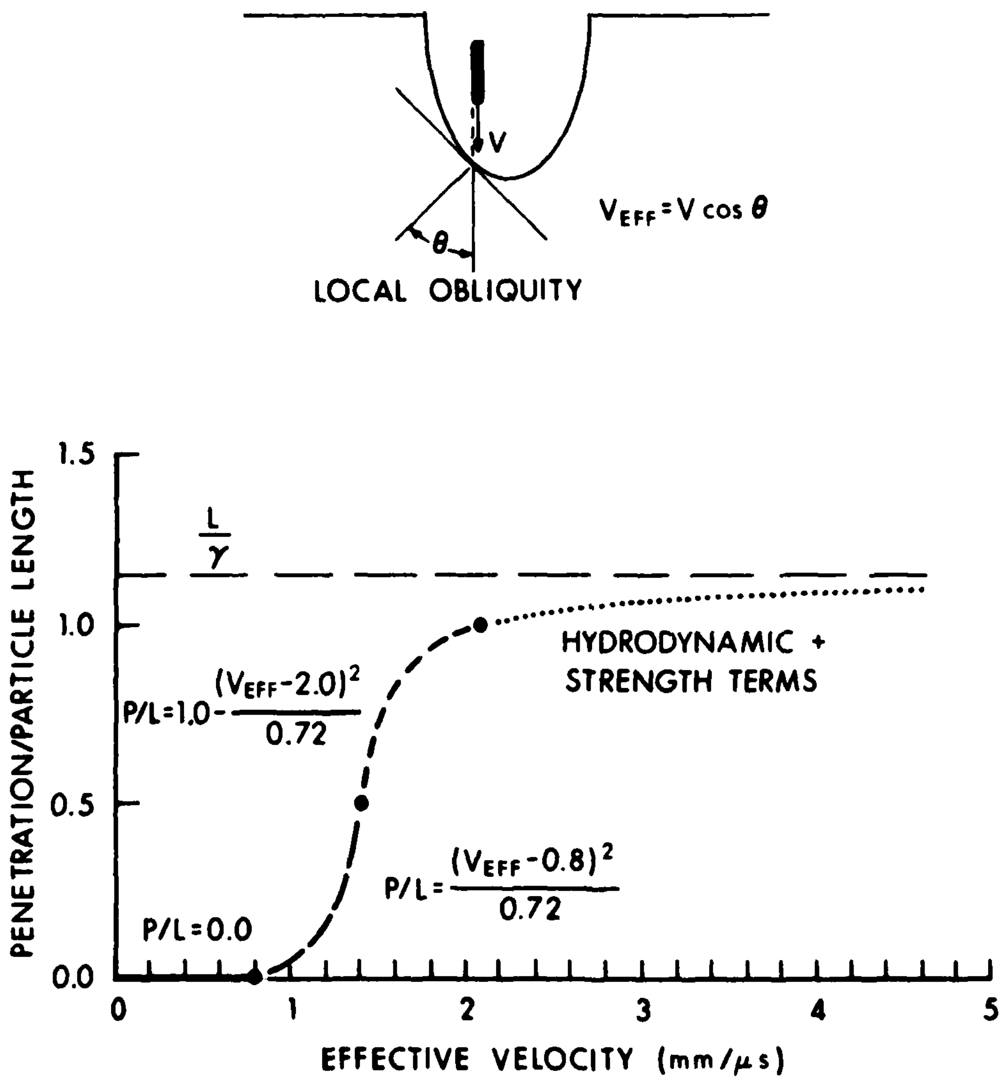

Figure 15. The Role of Effective Velocity in Penetration Calculations Involving Copper Jets Against Steel Targets

The asymptotic approach is generated using the hydrodynamic equations, including strength terms. For effective velocities below 2mm/μsec, penetration rapidly decreases in a manner expressed in Figure 15 so that no penetration is induced when the effective particle velocity is lowered beyond .8 mm/μsec. Data for the effective velocity curve in the low velocity regime was gathered from work by Weirauch.[6] Impacts of this nature may be the source of particle residue shown by Simon and DiPersio[7] to accumulate at the bottom of the hole profile. PENJET, however, does not consider this type of interference.

VI. APPLYING THE CODE TO DATA

Given a set of digitized radiographic data, PENJET will go through all of the mentioned calculations for each digitized particle of the jet to eventually create a three-dimensional hole profile for a given round at a given standoff. If the code is told to use the data of a given round to perform penetration calculations at a variety of standoffs, a theoretical penetration standoff curve can be generated for each round. This curve is, of course, only valid for a particular round. Thus, each generated curve is as individual as the data from which it was generated, and does not, in general, pertain to all rounds of the same type.

The code has both its good and bad aspects. A major consequence is that tilt has no direct effect on the code's ability to calculate penetration. This happens because tilt does not misalign the particles. Rather, it only redefines the charge axis. The particles still drift with respect to each other in the same fashion despite measurements including tilt. Much emphasis was previously placed on tilt for the reason that it would be advantageous to obtain drift distributions unbiased by tilt. In terms of the penetration calculations, though, tilt of and by itself has no effect.

Tilt does, however, indirectly affect the situation in terms of reference drift calculations. As relative drift velocity (as calculated from the radiographs) is the superposition of tilted and actual drift, abnormal relative drift distributions can occasionally result depending on how the two components of measured drift interact with each other. Correspondingly, abnormal relative drift distributions lead to abnormal extrapolations of reference drift, thus making the calculated reference drift suspect. After all, the calculation of reference drift is only an educated approximation: Direction of the drift is based on jet particle orientation, while magnitude of drift velocity is based on Equation (9). Therefore, unlike relative drift computations, which are as good as accuracy of measurement, reference drift is only as good as the governing assumptions. Thus, the poorer the approximation at reference drift, the poorer the quality of penetration calculations.

---

6 *G. Weirauch, "The Behavior of Copper Pins Upon Impacting Various Materials With Velocities Between 50 m/s and 1650 m/s," (Doctoral Thesis) University of Karlsruhe, 1971.*

7 *J. Simon, R. DiPersio, "Experimental Verification of Standoff Effects on Shaped-Charge Jet Cutoff in Solid Targets," Ballistic Research Laboratory Memorandum No. 1976, May 1969 (AD 854396).*

Another drawback to the code results from the radiographs themselves. The code can only analyze particles that have been digitized. In most radiographs some portion of the jet that is visible has not yet particulated. Attempting to separate the continuous jet into digitizable portions has met with some success, though likely at the cost of accuracy of particle length, since the continuous particles are still stretching when digitized. Also, most radiographs don't even contain the complete jet, for there is still jet matter that hasn't reached the plane of the film by the time it is exposed. Thus, there is no way to digitize these particles. For the rounds studied, it is estimated that over 40% of the jet was routinely nondigitizable.

To what extent the ability to digitize particles affects the penetration code predictions depends on the quality of the jet. In fact, the poorer the jet is, the less predictions are affected. If the undigitized particles drift far enough off course from the front portion of the jet, they will never make it to the bottom of the hole profile to add to penetration. In this situation, calculations based only on the particles digitized should produce results compatible with calculations involving all particles. Since distance of deviation is directly proportional to time in flight which is directly proportional to standoff, longer standoffs will also decrease the penetration effectiveness of the rear of the jet. Thus, penetration predictions at short standoff are subject to unavoidable error since the undigitized jet portion is still capable of increasing jet penetration. The fact that the penetration effectiveness of the jet rear is predicted to decrease with increasing standoff correlates with the DSM concept of minimum jet velocity increasing with standoff. [3]

Having kept these reservations in mind, the results of the code based on data from four rounds are illustrated in Figures 16-19. The only factor governing the choice of these particular four rounds was penetration; that is, rounds were chosen with varying penetrations ranging from poor to good. The code was run at standoff increments out to 38 CD. The actual rounds were fired at 24 CD standoff to allow radiography, and the actual penetrations achieved are shown on each of the graphs as a single datum. Steplike variations in the code's predictions result because of the discreteness of the impacting particles: Either a particle made it to the bottom of a hole profile or it did not. Major fluctuations in the code predictions can be taken to imply uncertainty in the jet performance. Uncertainty as to whether two or three given particles make it to the bottom of the hole profile can create penetration variations in excess of 1/2 CD. A curve was drawn to fit the code's predictions on each of the rounds, though a band width of uncertainty should be realized as well. This curve is PENJET's prediction of penetration, assuming that one could fire the exact same round over and over again at various standoffs. Since we know that the predictions at short standoff are inaccurate due to nondigitizable jet, the code's predictions on Figures 16-19 are generally unreliable below 10 CD. The curve, however, should be valid at the standoff of 24 CD at which the rounds were actually fired.

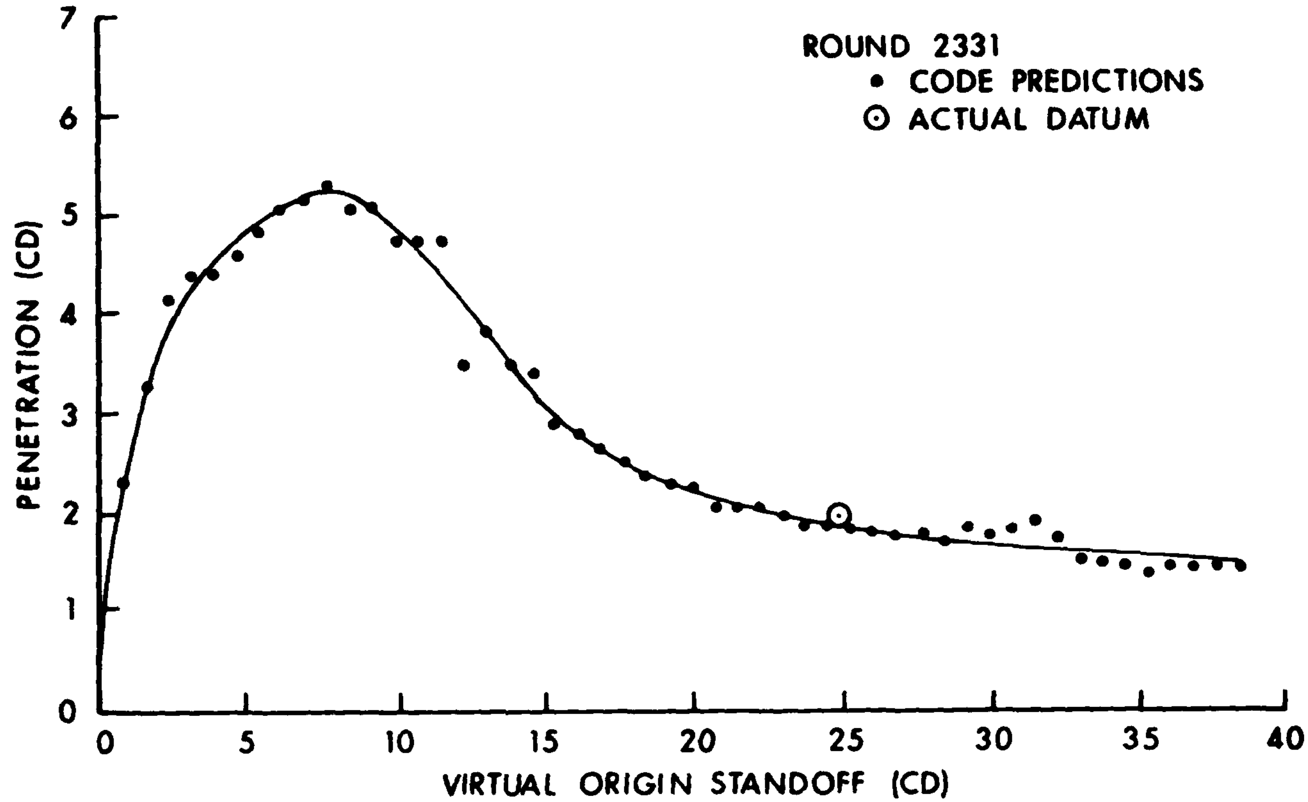

Figure 16. Analysis of Round 2331

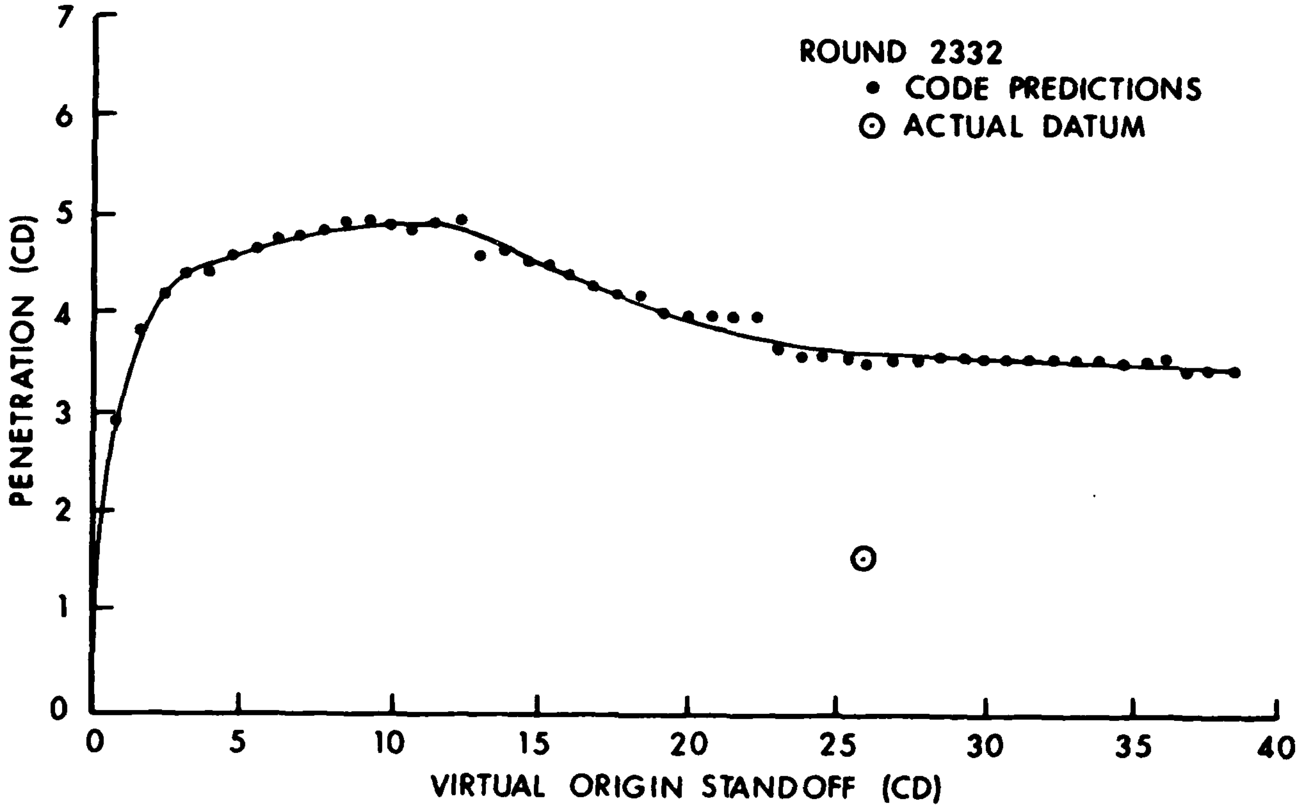

Figure 17. Analysis of Round 2332

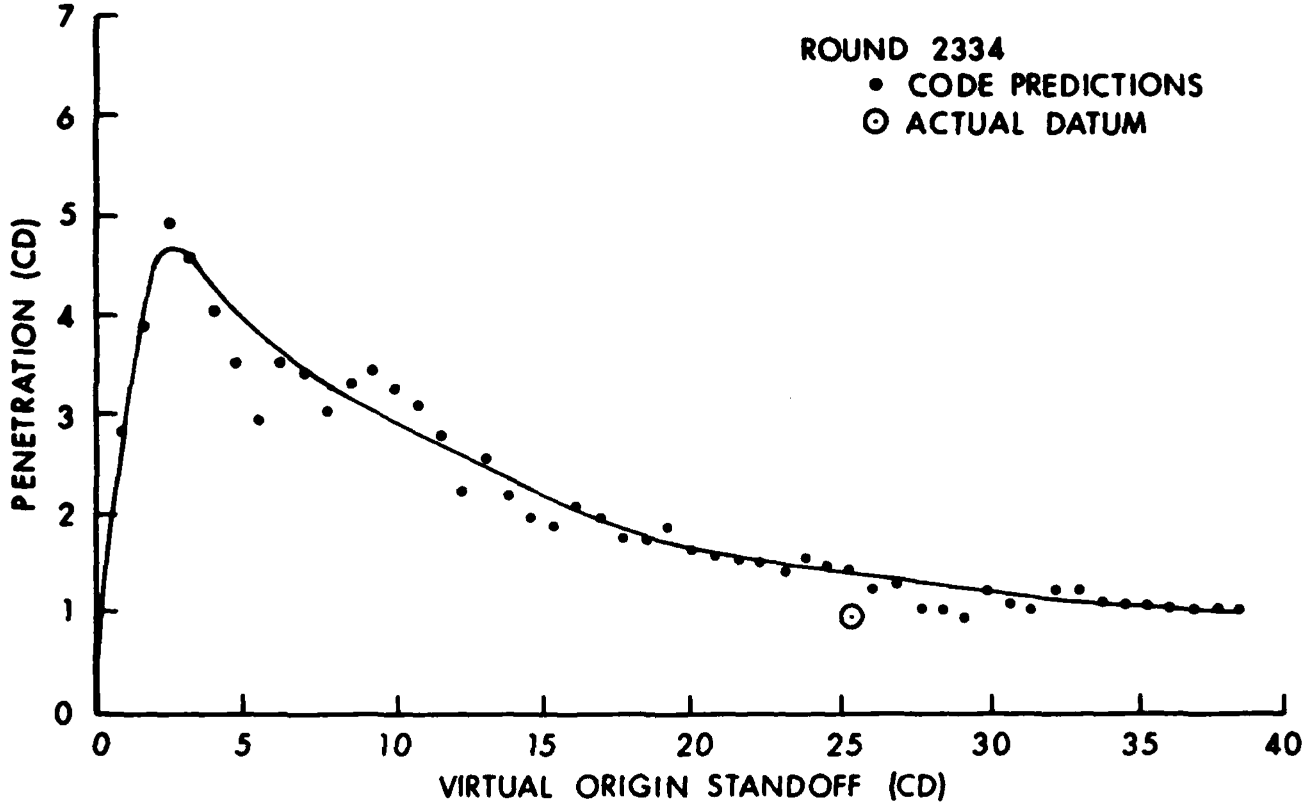

Figure 18. Analysis of Round 2334

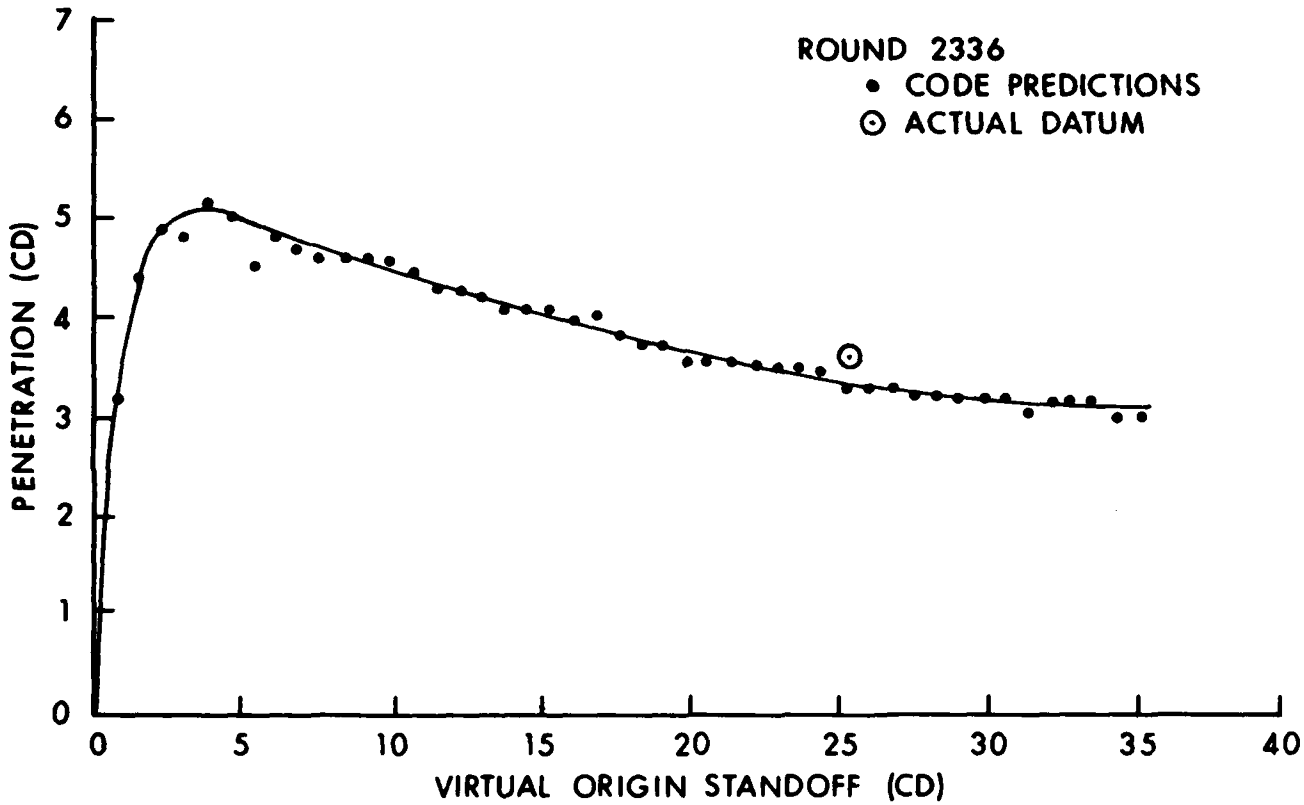

Figure 19. Analysis of Round 2336

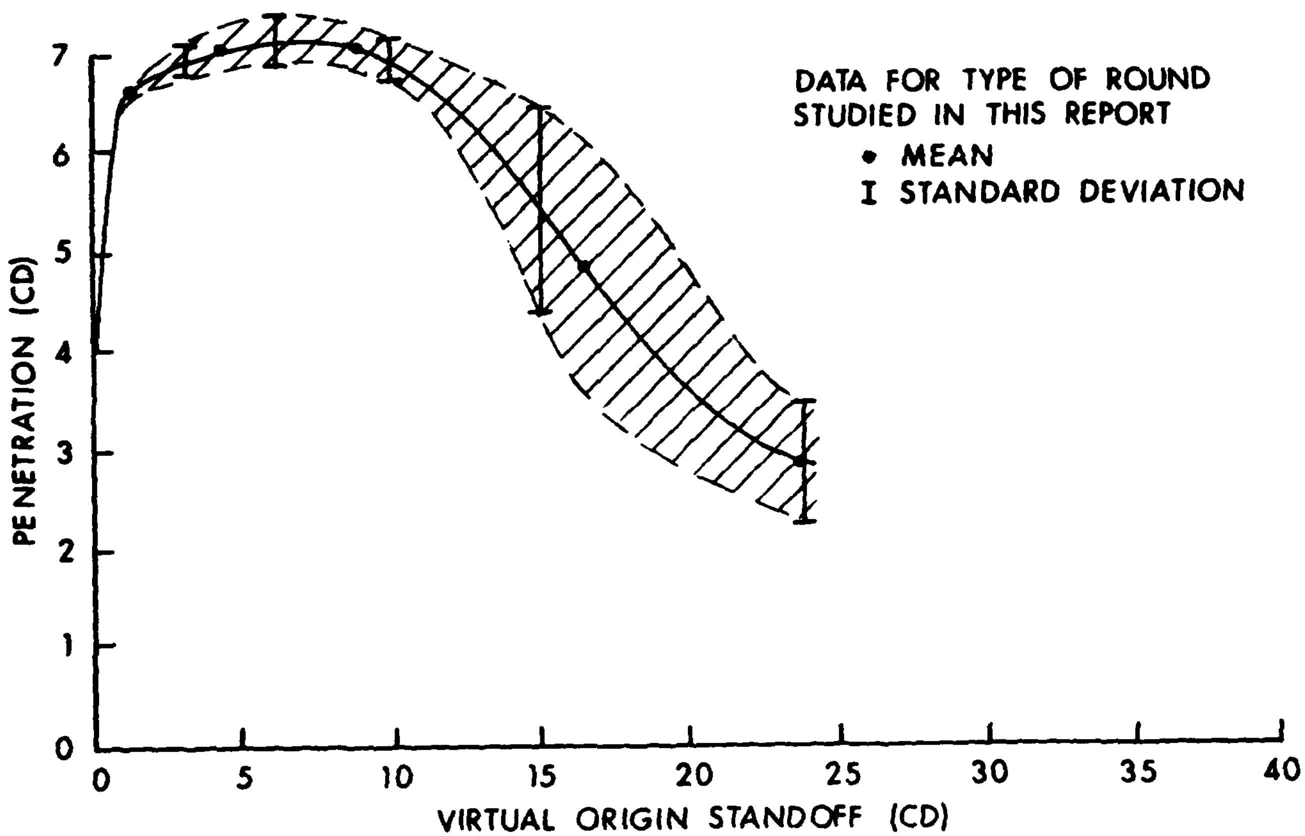

Figure 20. Routine Performance for Type of Round Analyzed

All of the codes's predictions were in reasonable agreement with experiment except for Round 2332. Upon studying this round for possible causes of discrepancy, it was noted that the round uniquely had what shall be called a switchback angular spiral. This falls into the category of abnormal relative drift distributions. Most jets contain drift distributions such that the jet particles spiral in only one direction (either clockwise or counterclockwise) throughout the jet. Figure 5, for example, shows a jet spiralling counterclockwise from jet tip to tail. A switchback angular spiral is one in which one part of the jet spirals in one direction, while the subsequent portion of the jet spirals in the opposite direction. Switchback is thought to be a product of abnormal tilt/drift combinations such that subsequent computation of reference drift might be quite inaccurate. As set forth before, an inaccurate reference extrapolation leads to inaccurate penetration calculations.

Figure 20 shows how the actual weapon routinely performs. In order to test whether PENJET could predict the average penetration at standoffs near the peak performance of the round, a radiograph containing a complete and fully particulated jet would be required for digitization. As mentioned previously, no available radiographs fulfilled these requirements. A radiograph was obtained, however, of a complete jet which was not fully particulated. Though not completely digitizable, the presence of a complete jet greatly facilitated estimation of many jet parameters (e.g. velocity of jet rear, drift with respect to jet rear, and total jet length). By this means, the rear of the jet which was not digitizable could be simulated into particles based on analysis of the radiograph containing the continuous jet rear.

Figure 21 shows the PENJET prediction of the round that includes the jet rear simulation. The actual datum as well as optimum performance for this type of round are included in order to put PENJET calculations in perspective.

The importance of a complete jet at short standoff is shown in Figure 22. The penetration standoff curve for Round 2331 is shown here. Superimposed upon it are curves showing the amount of residual penetration resulting from different fractions of the complete jet. The points at which the curves meet signify that the number of particles producing the superimposed curves are also the same number of particles producing the total residual penetration at that point. For example, PENJET's predictions at 11.5 CD standoff imply that predicting penetration using 40 particles would be just as accurate as using 51 particles. Anything less than 40 particles at that standoff would, however, produce inaccurate results. For the 24 CD standoff at which the round was actually fired, less than 20 digitized particles would be required for an accurate description of penetration. At short standoff, however, even 51 particles do not completely describe the penetration capabilities of Round 2331. Estimates are that below 8 CD standoff, particles beyond particle 51 were also capable of adding to penetration. For better quality rounds, though, as illustrated by Round 2937 in Figure 23, more particles are required even at longer standoffs to accurately describe penetration. For example, more than 50 digitized particles would be required for standoffs out to 25 CD for this particular round.

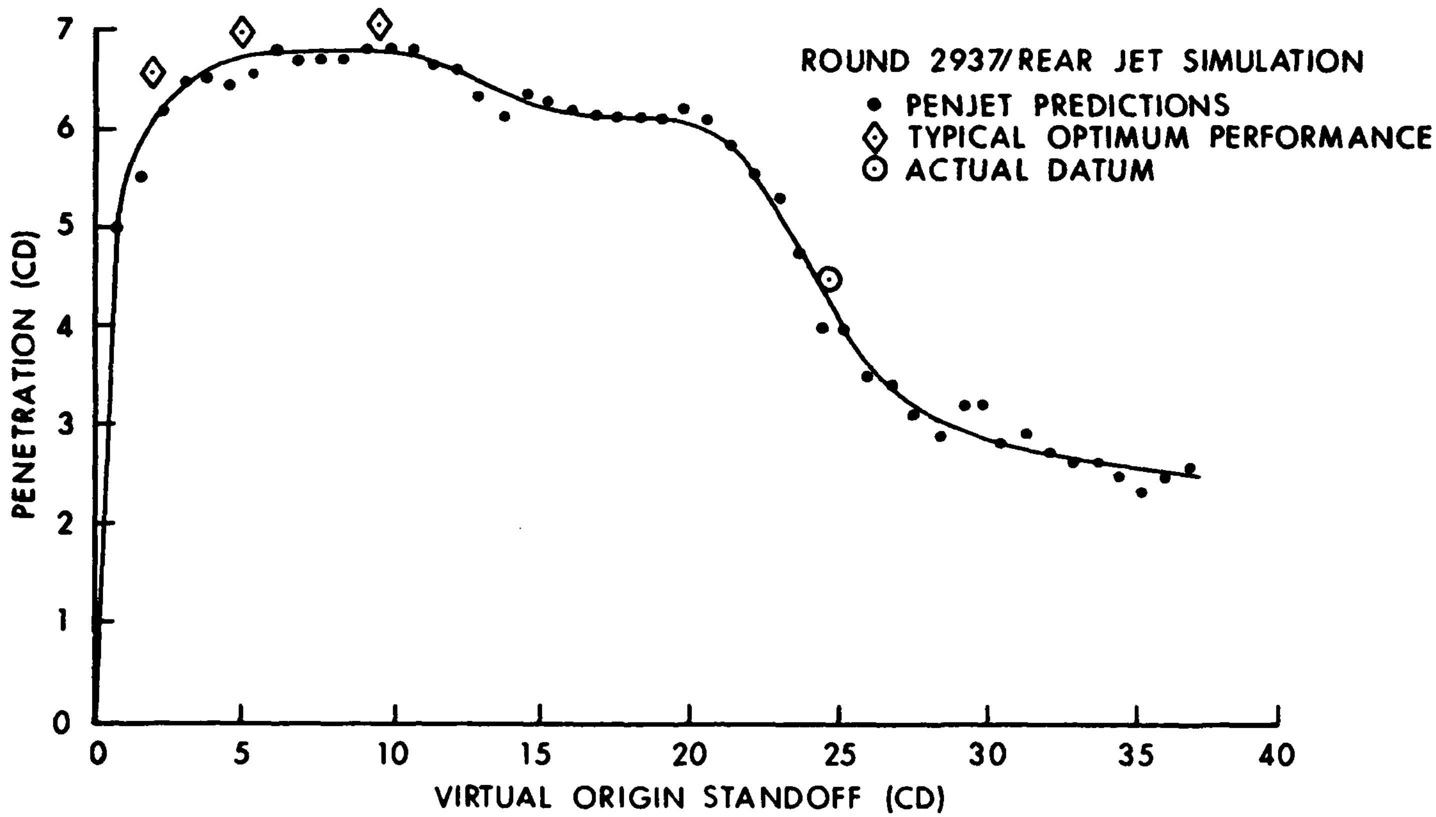

Figure 21. Analysis of Round 2937 with the Included Jet Rear Simulation
Note: Optimum Performance Data Transferred from Figure 20.

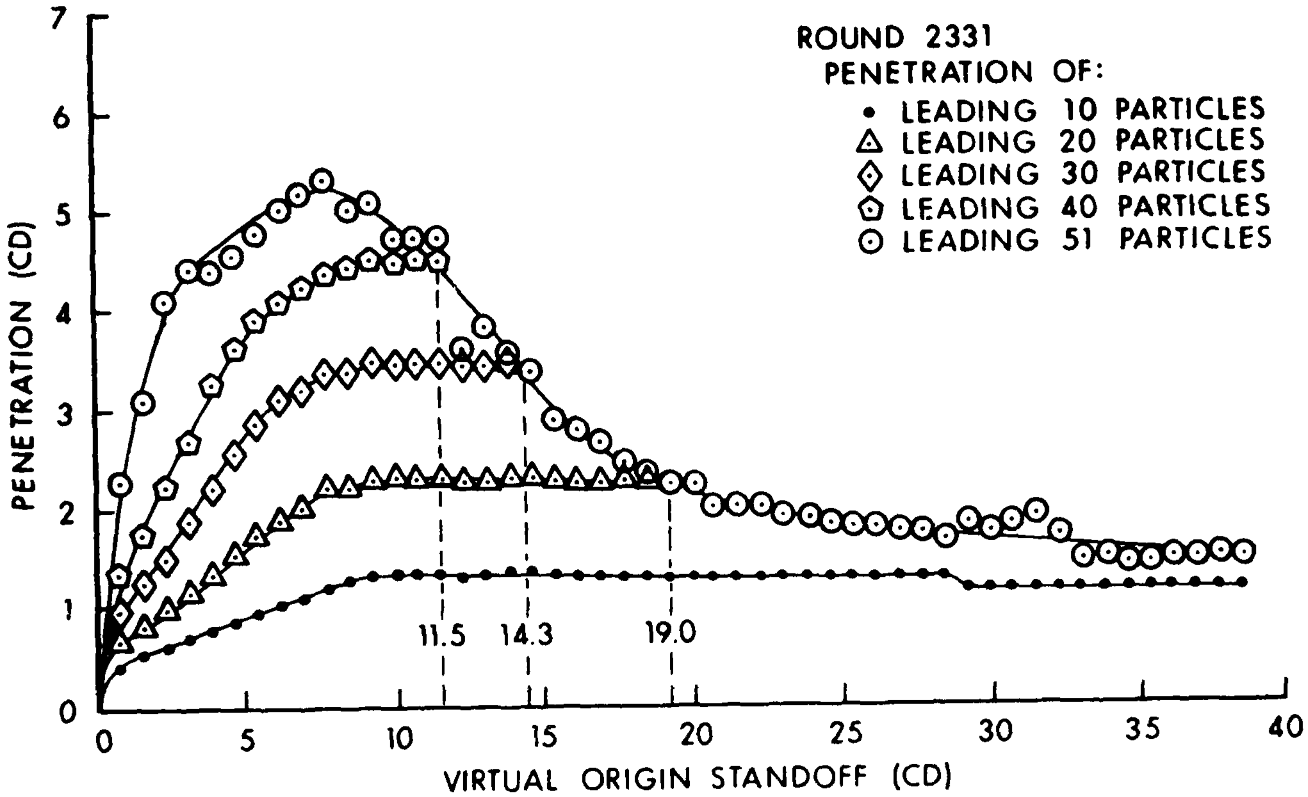

Figure 22. Penetration Capability of Distinct Jet Portions of Round 2331

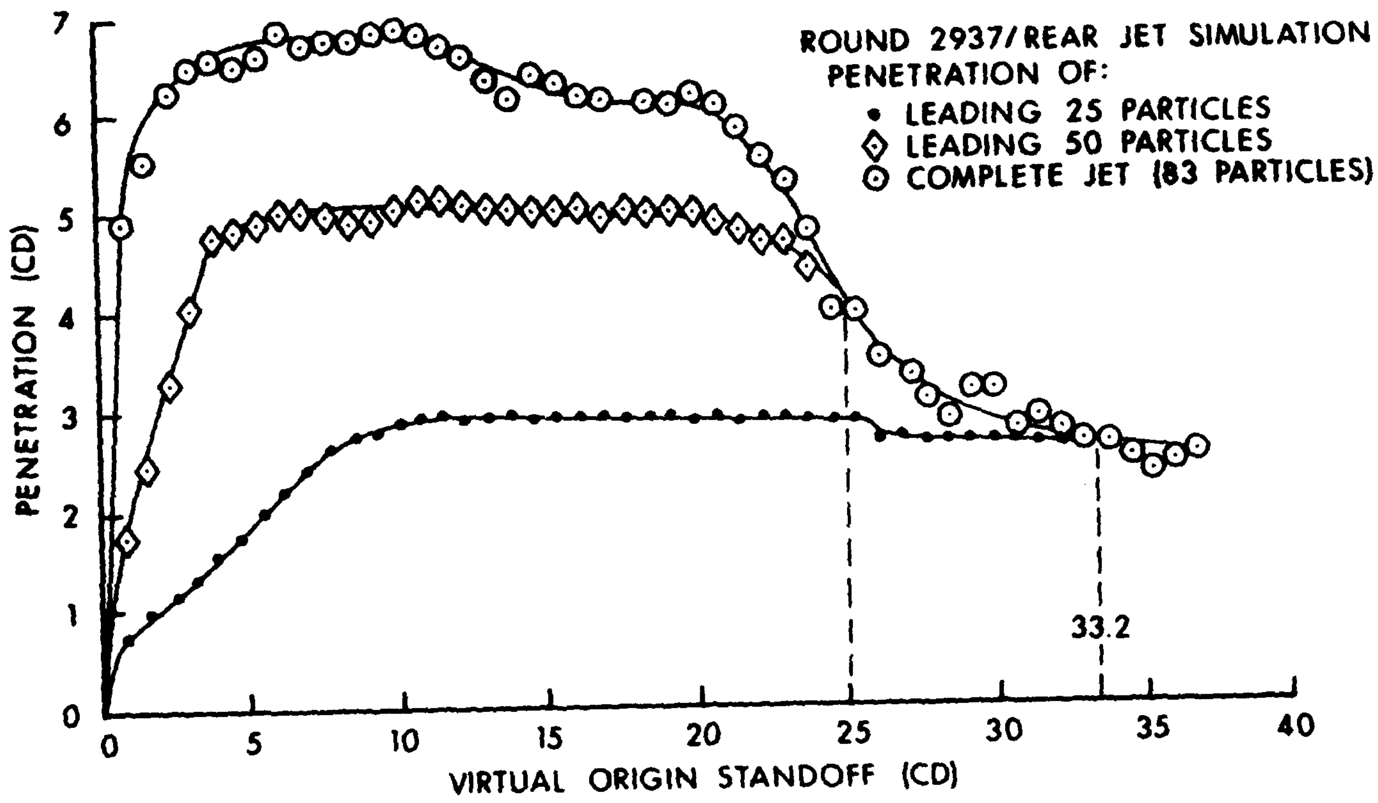

Figure 23. Penetration Capability of Distinct Jet Portions of Round 2937

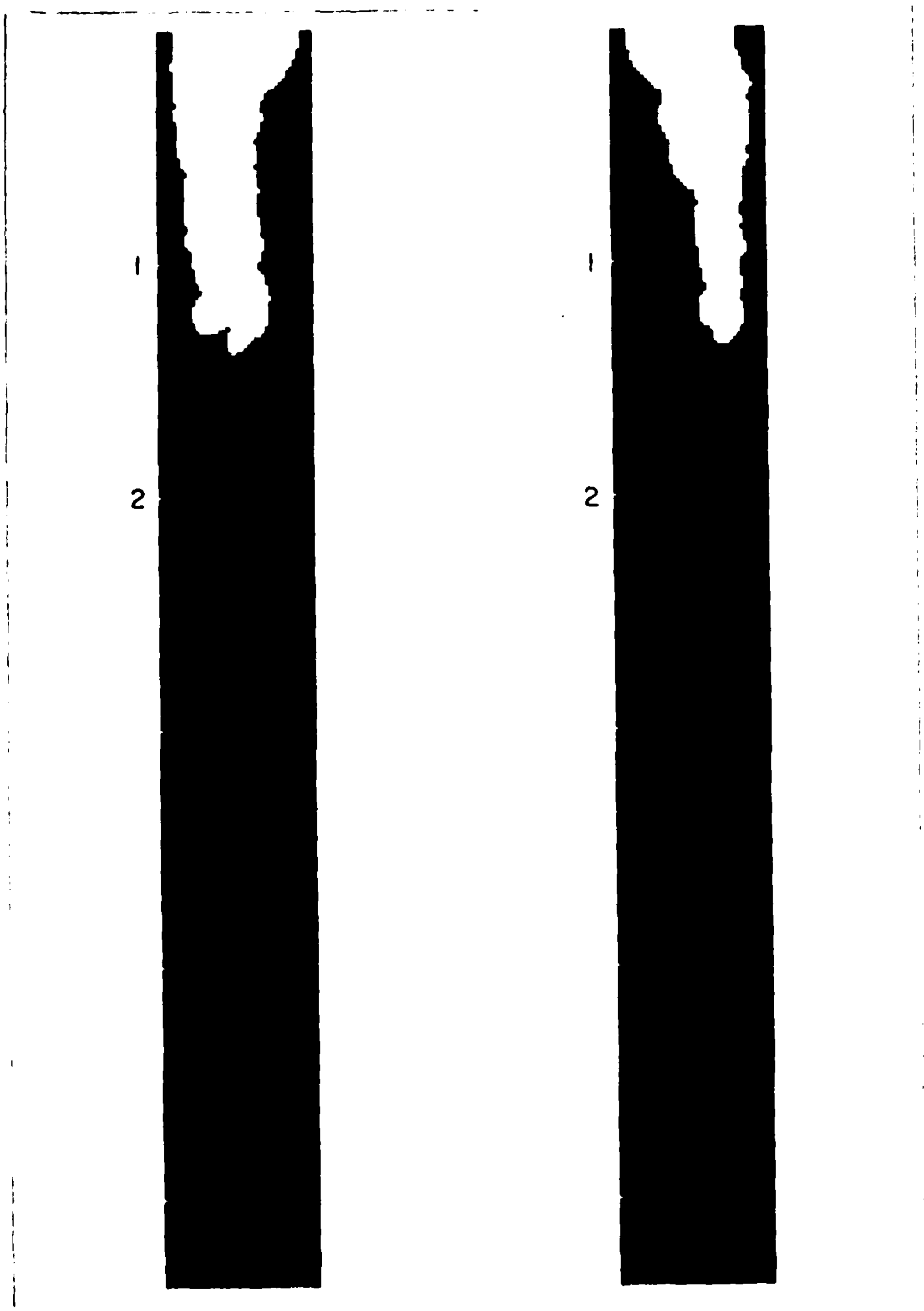

Figure 24. PENJET Predictions of Hole Profile for Round 2334 at 23 CD Standoff. Penetration in Cone Diameters.

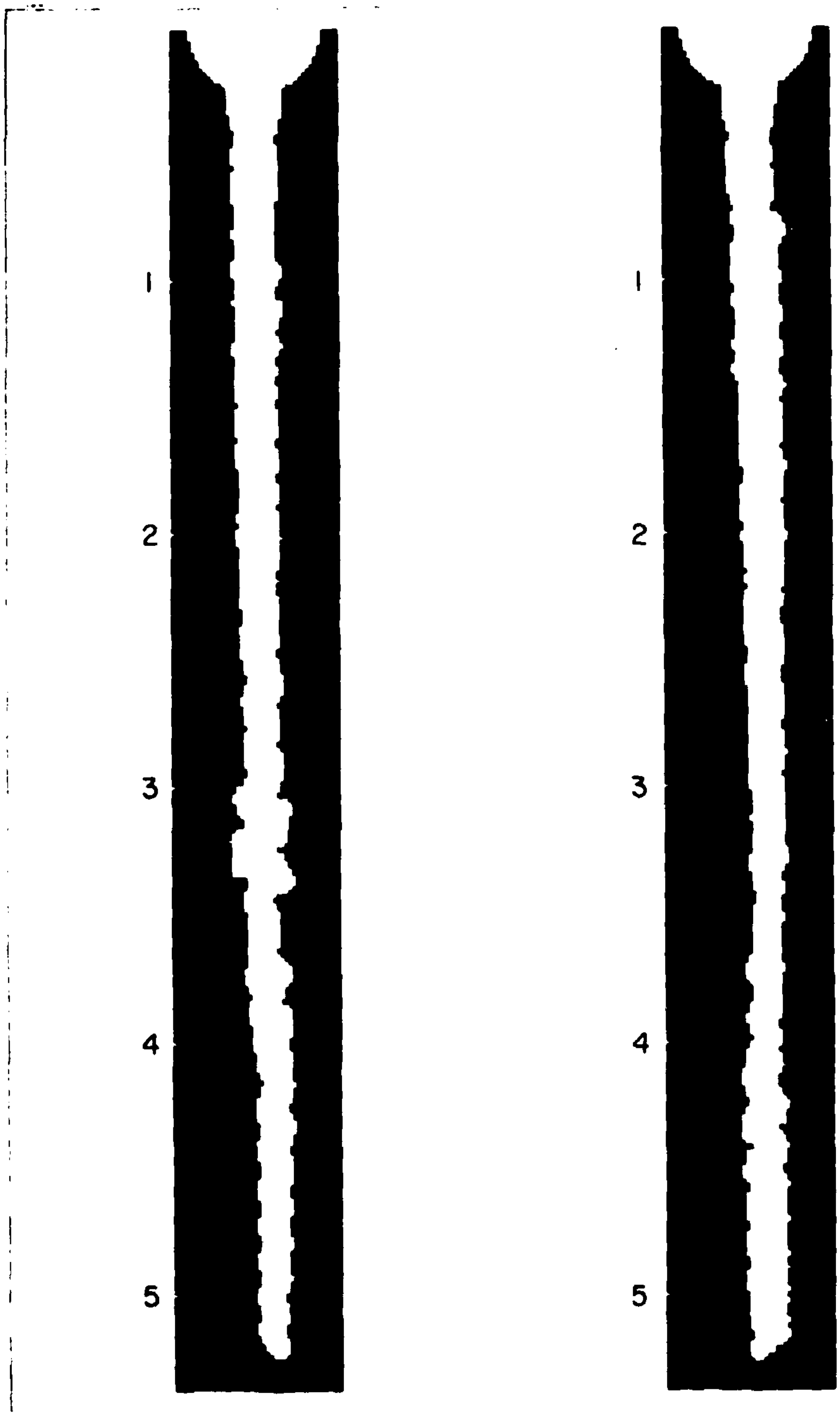

Figure 25. PENJET Predictions of Hole Profile for Round 2937 at 23 CD Standoff. Penetration in Cone Diameters.

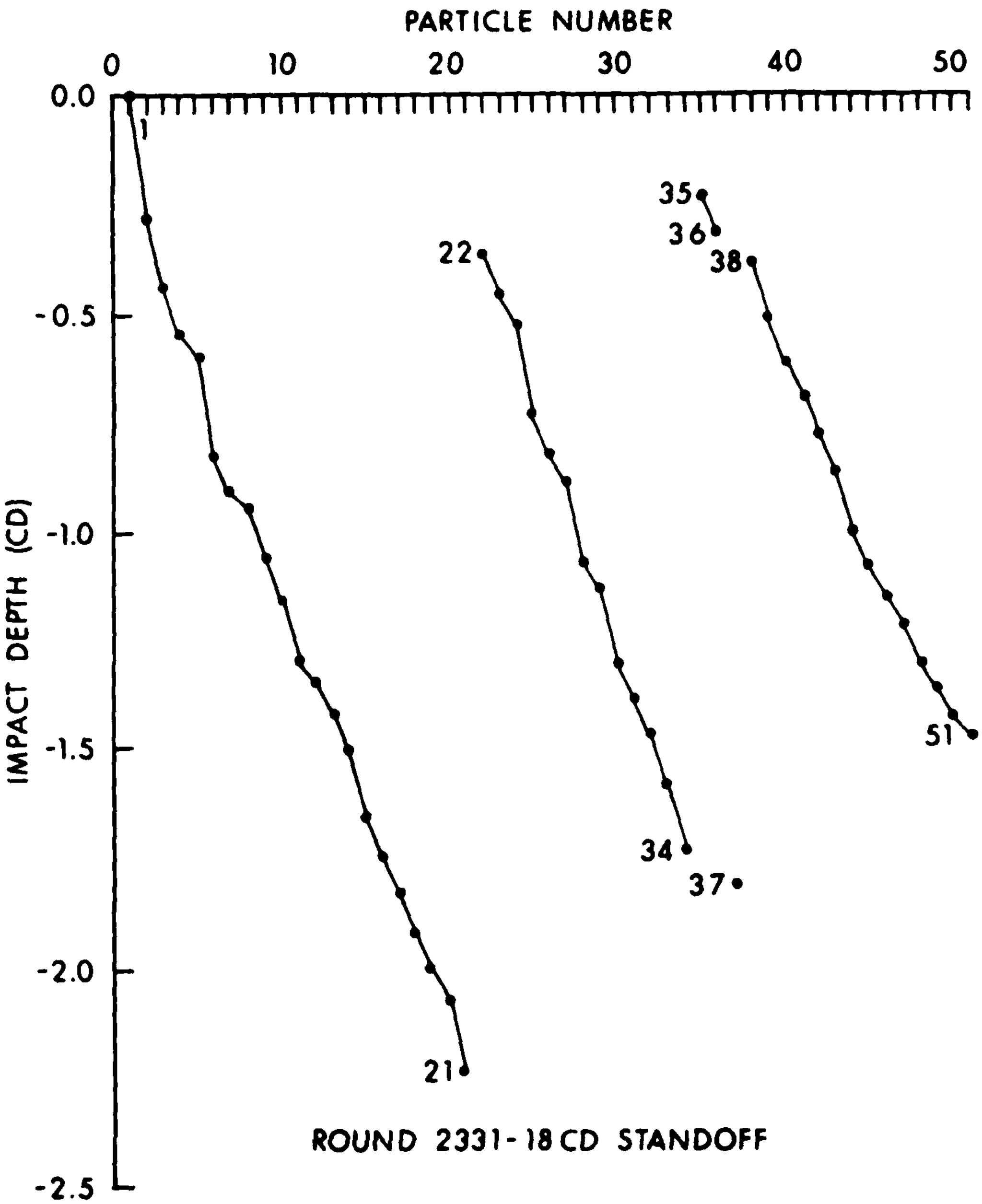

Figure 26. Code Predictions of Rear-Jet Ineffectiveness Due to Side Wall Impacts of Drifting Particles

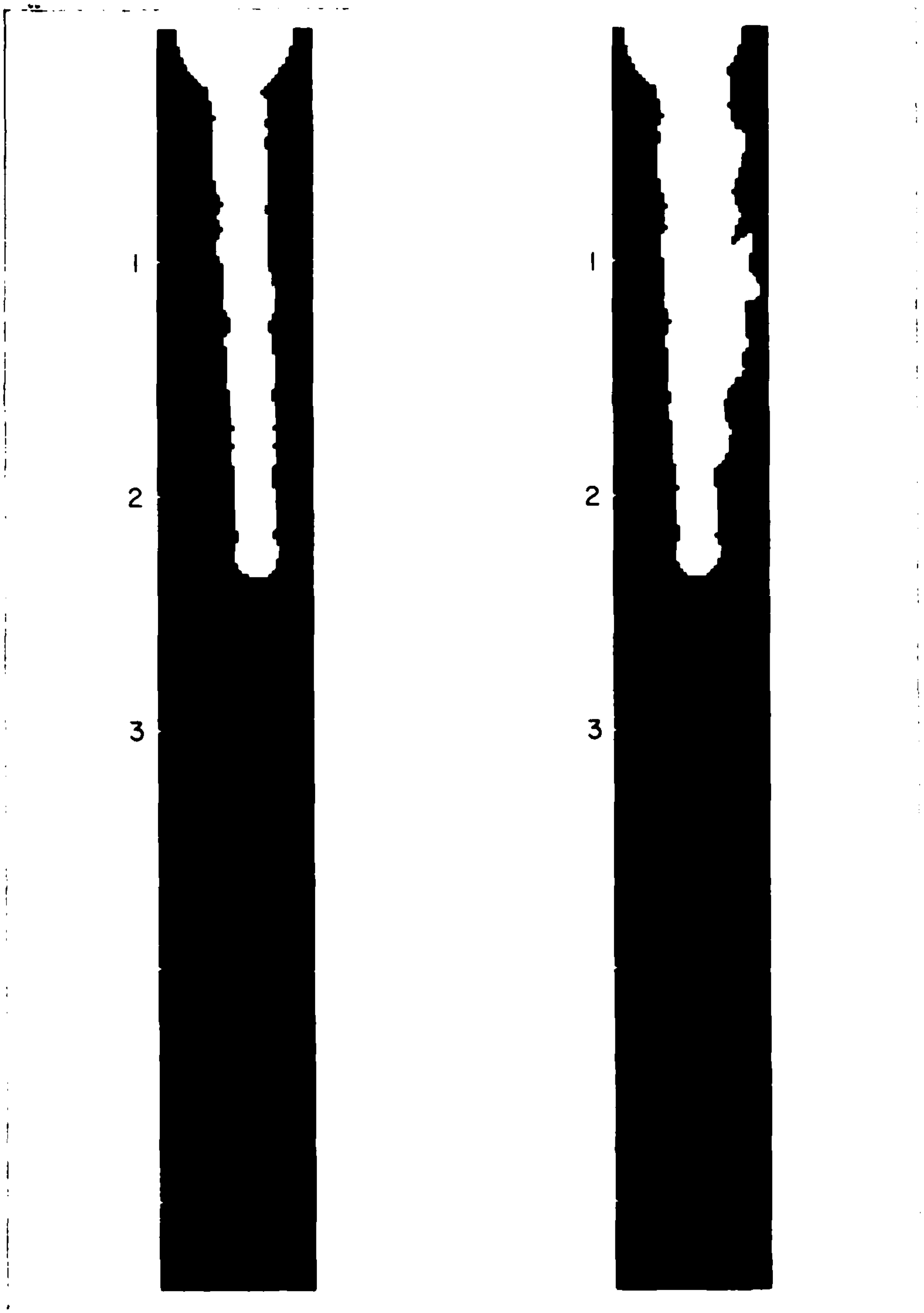

Figure 27. Orthogonal Views of Projected Hole Profile of Round 2331 at 18 CD Standoff as Predicted by PENJET. Penetration in Cone Diameters.

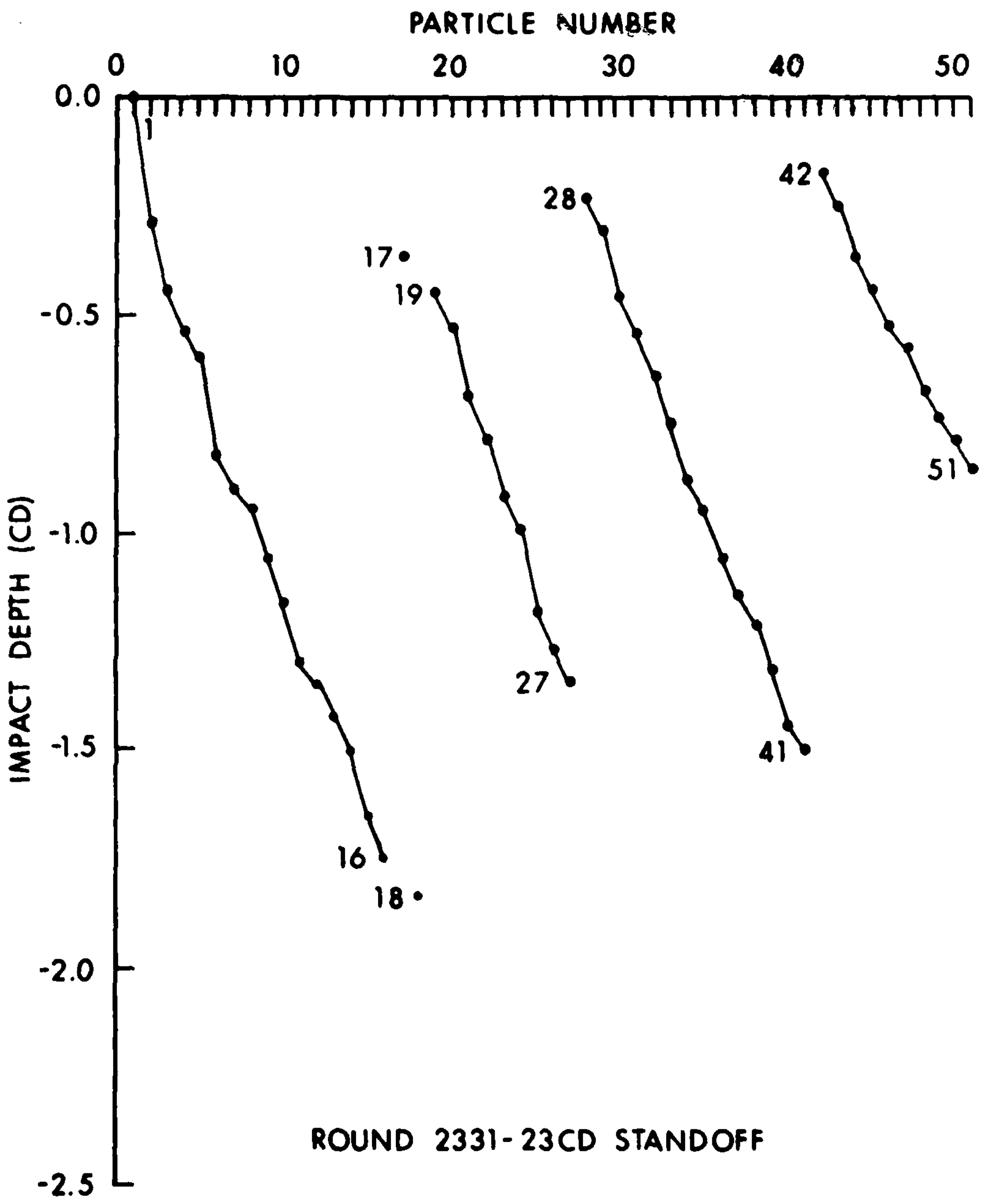

Figure 28. Increase of Side-Wall Impacts Predicted at Longer Standoffs

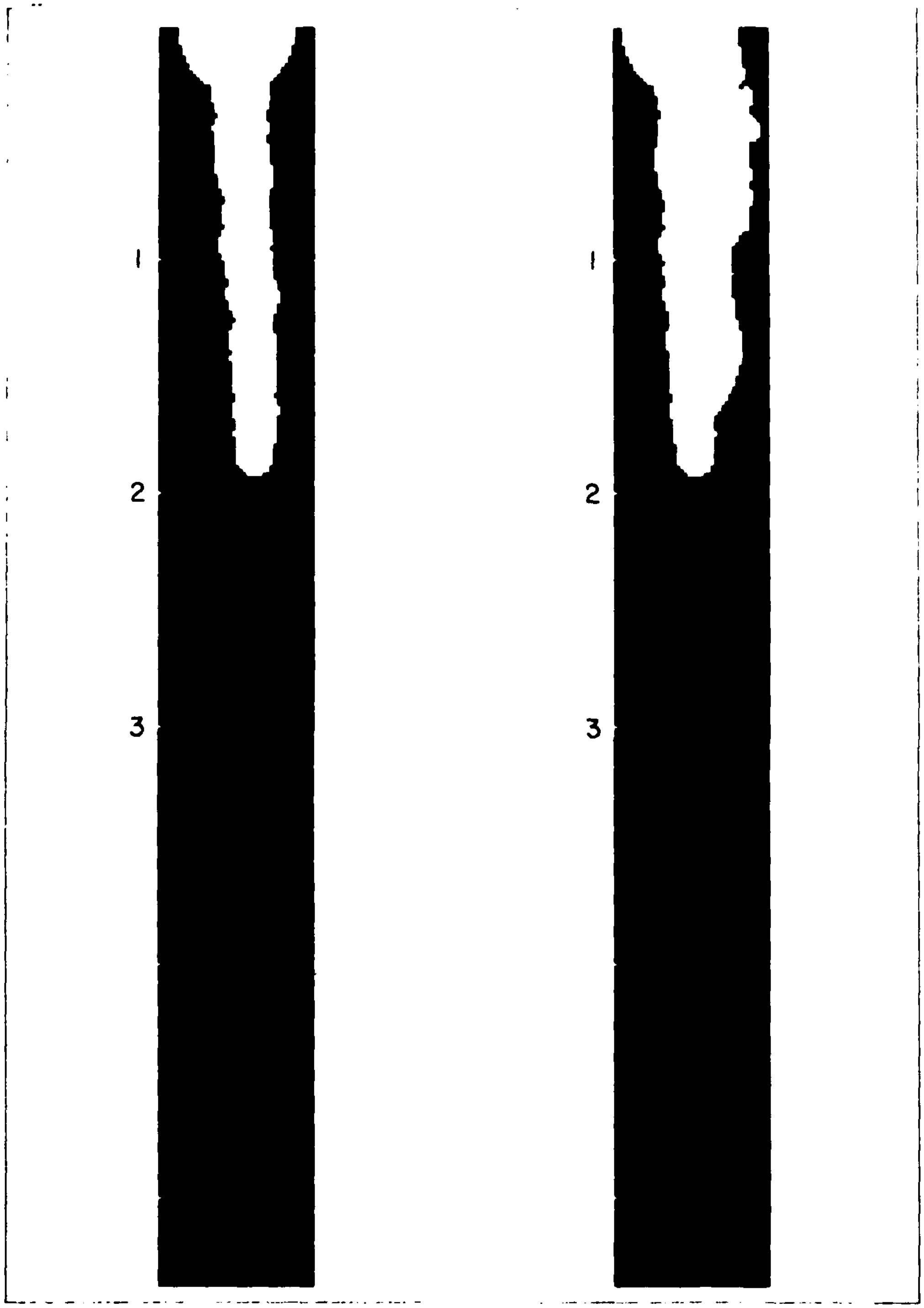

Figure 29. Orthogonal Views of Projected Hole Profile of Round 2331 at 23 CD Standoff as Predicted by PENJET. Penetration in Cone Diameters.

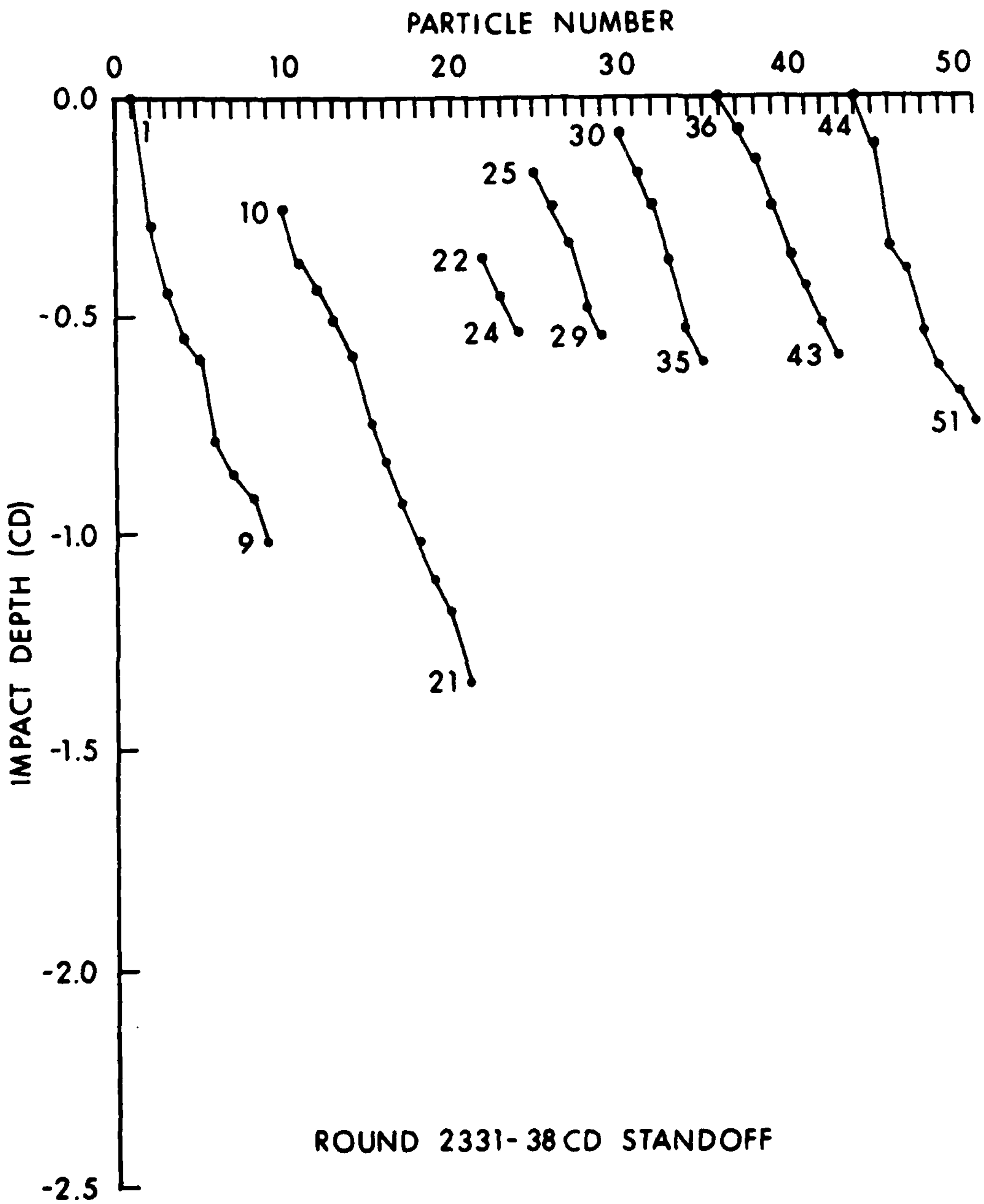

Figure 30. The Effect of Side Wall Impacts is Not Only to Decrease Penetration, But to Widen Crater.

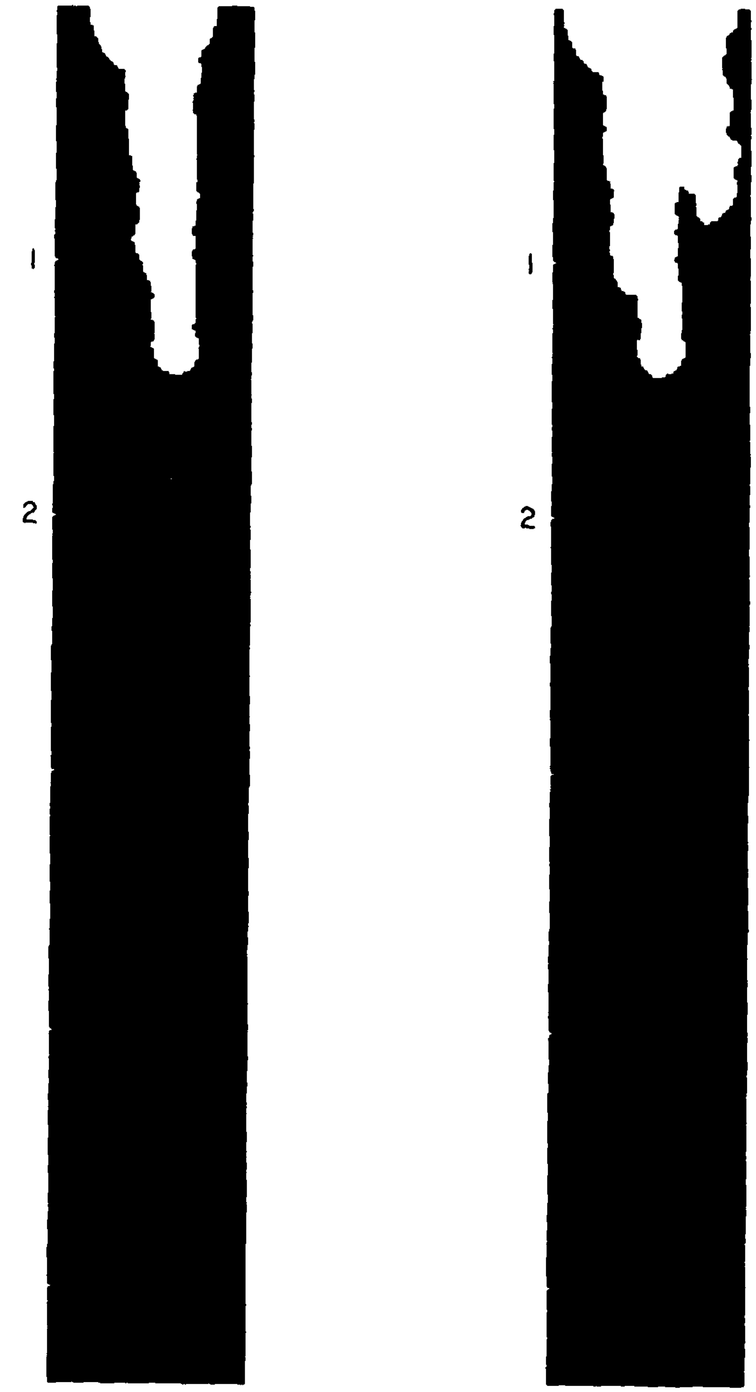

Figure 31. Orthogonal Views of Projected Hole Profile of Round 2331 at 38 CD Standoff as Predicted by PENJET. Penetration in Cone Diameters.

Besides showing a semblance of agreement between code and experiment, Figures 16-19 show that drift alone can easily account for rapid decreases in penetration as is often experienced by rounds at extended standoffs. The process by which penetration is decreased is one of sidewall impacts. This process was briefly mentioned before as a phenomenon which sometimes renders a particle ineffectual. The majority of sidewall impacts, though, are not so oblique as to disrupt penetration; most sidewall impacts go into creating wider hole profiles.

As an example of the devastating effects of drift velocity on jet penetration, a comparison of PENJET's hole profile predictions is shown for two separate rounds in Figures 24 and 25. The plots represent orthogonal views of the target block as described by PENJET. Both sets of calculations were performed at the same standoff (23 CD). The stark contrast of jet performance is noted not only in terms of depth of penetration, but also in terms of crater width. Sidewall impacts do not occur until much later in the penetration process for Round 2937, thus allowing more of the jet to contribute to the overall penetration.

Figure 26 is PENJET's prediction as to where in the hole profile each particle of Round 2331 strikes the target block at 18 CD standoff. Note that particle number is in order of formation. (Jet tip is particle 1.) It is seen that once a particle is blocked from reaching the bottom of the hole, it will usually begin the widening process somewhere up the profile. Subsequent particles try to work their way back down again. This process continues until no jet is left with which to penetrate the target. A plot of the hole profile as generated by PENJET is shown in Figure 27 as two orthogonal views of the target block. Graphs and plots for the same round are shown again at longer standoffs in Figures 28-31. It is seen that penetration is progressively lower because sidewall impacts occur earlier in the penetration process. Consequently, crater diameter progressively increases at longer standoffs. Thus, for Round 2331 at a standoff of 23 CD the total penetration capability of the jet as predicted by PENJET is contained within the first 18 particles.

The profile at 38 CD sharply illustrates the effects of drift velocity on jet penetration. The spread of the particles was so great as to cause the beginnings of a dual crater within 1 CD of the target surface. Thus, the ineffectiveness of the jet rear is seen. Any nondigitized portion of Round 2331 would probably produce its penetration in the vicinity of the particle 51 crater, far from the point of maximum penetration.

Thus, the decreases in penetration as predicted by PENJET are due mainly to the presence of drift velocities among the particles. Drift causes scattering of the particles and eventually, at some critical standoff, elimination of the particles from the crater deepening process via the mechanism of sidewall impacts.

VII. CONCLUSIONS

The ability to compute drift velocities for the particles of a shaped-charge jet is thought to be significant. In its own right, quantification of drift velocity aids in understanding the nature of the nonideal jet. A degree of imperfection may also be placed upon the jet in hopes of classifying a jet with regard to its quality.

The concept of how a jet penetrates is better understood when drift velocity is considered in the penetration picture. The process of sidewall impacts as a hinderance to penetration can be verified by inspection of actual target blocks. This process is reminiscent of the jet cutoff velocity which varies with standoff as proposed by Dipersio, Simon, and Merendino,[3] in that the velocity of the particle striking deepest in the hole profile can be considered a cutoff velocity with respect to jet penetration. Implications here are that a jet could approach ideal penetration had drift velocity not been present. Larger craters would also make jets more insensitive to drift. Weaker targets allow for a wider crater for a given jet particle. Thus, the reduced probability of sidewall impact would allow greater penetration.

Compared to armor, a target of mild steel hydrodynamically should not affect the penetration of a given jet. It will affect penetration, however, when drift velocity is present in the jet. DiPersio and Simon[8] verified this experimentally by firing jets into steel targets of varying hardness. Increasing crater size could alternately be accomplished by means of increasing the jet's energy. If dynamic impact did not induce additional drift in the jet, projecting the round into the target, as is the case under field conditions, should produce greater penetration than the static detonation of the same round. This cannot be verified experimentally, however, due mainly to the complexity of dynamic impact. Besides possessing possible yaw and pitch, the dynamic round is moving with respect to the target during the jet formation process. This relative motion can manifest itself in the form of drift. Dynamically detonated rounds do, however, create wider craters than their static counterparts as expected.

It is suggested that future investigations attempt to analyze drift from the viewpoint of warhead causes. The first step in understanding penetration in terms of drift has hopefully been set forth in this report. The ability to analyze drift as a function of the warhead would be the link between the imperfect warhead and nonideal penetration. Eventually, the possibility exists where warhead tolerances may be used to place limits upon the drift velocity distributions for a round so that penetration might be expressible as a function of charge tolerances.

---

[8] *R. DiPersio, J. Simon, "The Effect of Target Hardness on the Penetration Capability of Shaped-Charge Jets," BRL Report No. 1408, July 1968 (AD 838991).*

ACKNOWLEDGEMENTS

The author wishes to acknowledge the following members and emeriti of the Warhead Mechanics Branch of the U.S. Army Ballistic Research Laboratory for their encouraging support of this analysis: R. Jameson, M. Lampson, and J. Simon for technical consultations; V. Kucher for assistance rendered regarding computer related procedures; M. Scarborough and B. Simmons for having radiographs digitized and ready for use as computer data.

REFERENCE LIST

1. J. Blische, B. Simmons, "A Method for Reducing Data from Radiographs of Shaped-Charge Jets," BRL Report ARBRL-TR-02330, Jun 81 (AD A102770).

2. K. N. Kreyenhagen, J. E. Ferguson, R. R. Randall, J. P. Joyce, "Special Explosive Projectors," Proc. 6th Symposium Hypervelocity Impact, Vol. I (Held Cleveland, Ohio, April 30-May 2, 1963).

3. R. DiPersio, J. Simon, A. Merendino, "Penetration of Shaped-Charge Jets Into Metallic Targets," Ballistic Research Laboratory Report No. 1296, September 1965 (AD 476717).

4. E. Fitzgerald, Particle Waves and Deformation in Crystalline Solids, Interscience Publishers, New York, 1966.

5. J. Kineke, Jr. "An Experimental Study of Crater Formation in Metallic Targets," Proc. 4th Symposium Hypervelocity Impact, Vol. I (Held Eglin AFB, Florida, April 26-28, 1960).

6. G. Weihrauch, "The Behavior of Copper Pins Upon Impacting Various Materials with Velocities Between 50 m/s and 1650 m/s," (Doctoral Thesis) University of Karlsruhe, 1971.

7. J. Simon, R. DiPersio, "Experimental Verification of Standoff Effects on Shaped-Charge Jet Cutoff in Solid Targets," Ballistic Research Laboratory Memorandum No. 1976, May 1969 (AD 854396).

8. R. DiPersio, J. Simon, "The Effect of Target Hardness on the Penetration Capability of Shaped-Charge Jets," BRL Report No. 1408, July 1968 (AD 838991).

APPENDIX A

PROGRAM LISTING

AND

VARIABLE NAME DESCRIPTIONS

PRECEDING PAGE BLANK-NOT FILMED

The drift velocity and PENJET programs were written as direct additions to Blische's and Simmons' radiograph-data-reduction program (Reference 1) introduced in BRL Report 2330. Therefore, a listing of PENJET must be accompanied by the program which generates data for use within PENJET. The right-hand edge of the listing reveals where the statements in question originated. "GETREADY" are nonexecutable statements required for BRL Report 2330, PENJET, or both. "BRL 2330" is the bulk of Blische's and Simmons' program with minor revisions for PENJET applicability. "JETBREAK" is a revision for jet breakup calculations. "DRIFT" is used to calculate the drift distribution for a round while "PENJET" is the jet penetration program. The program is written in FORTRAN IV. An explanation of the program variables is inserted after the program listing.

It should be noted that even though Blische's and Simmons' program is versatile enough to run using data from only two X-ray flash exposures, PENJET is geared to the standard 3 flash setup and will require modifications to run otherwise.

Explanation for the program variable names found in the program segment identified as "BRL 2330" can be found in BRL Report 2330 (Reference 1). Should one wish to identify variables within the program segment "GETREADY," the other segments should be consulted, as all "GETREADY" variables are contained within other segments. All other significant variables are listed under their appropriate program segment.

PRECEDING PAGE BLANK-NOT FILMED

```
      PROGRAM MAIN(INPUT,OUTPUT,TAPE5=INPUT,TAPE6=OUTPUT)                GETREADY
      DIMENSION S1(100),S2(100),S3(100),VOL(100),XL(100),DIA(100),        GETREADY
     1V1(100),V2(100),V3(100),VEL(100),XMASS(100),XKE(100),SUMKE(100),    GETREADY
     2ELOD(100),XXL(100),SUML(100),IX(6),IY(6),ZX(6),ZY(6),               GETREADY
     3BREAK(100),SUMMAS(100),B(10000),DA(3),DB(3),XMAG(3)                 GETREADY
      DIMENSION AA(2,3),CC(2),RR(500),AF(500),SIG(2),TT(2)                GETREADY
      DIMENSION DS(3),THETA(100),VETRAV(100),T1(100),T2(100),T3(100),     GETREADY
     1          REF(3)                                                    GETREADY
      DIMENSION AVST(100),BETA(100)                                       GETREADY
      DIMENSION PHI(100),PHIR(100),VTABS(100)                             GETREADY
      DIMENSION EPS(6,100),WT(6)                                          GETREADY
      DIMENSION VX(100),VY(100)                                           GETREADY
      DIMENSION R(2)                                                      GETREADY
      DIMENSION VTB(100)                                                  GETREADY
      DIMENSION T(100),X(100),Y(100),Z(100),U(100),RADIUS(100),PEN(100),  GETREADY
     1          HVOL(100)                                                 GETREADY
      DIMENSION NCC(100)                                                  GETREADY
      DIMENSION ZSUB(100),PENT(100),PENMAX(100)                           GETREADY
      DIMENSION V(100,3),VM(100),VA(100,3),VAM(100),VP(100,3),VPM(100),   GETREADY
     1          RGRAD(100,3),RGM(100),GRAD(100,3),AR(100,3),PR(100,3)     GETREADY
      DIMENSION RL(100),RVEL(100)                                         GETREADY
      DIMENSION OL(100),KVAL(100),TAU(100)                                GETREADY
      DIMENSION TP(100),RD(100)                                           GETREADY
      REAL KD12,KD23,KD13                                                 GETREADY
      REAL INCR                                                           GETREADY
      DIMENSION SA(10),SB(10),SC(10),SD(10),SE(10),SF(10),SL1(10),        GETREADY
     1SL2(10),SL3(10),ST(10),L1(100),L2(100),L3(100)                      GETREADY
      DIMENSION P(100),TOTP(100),SUMDIA(100),SUMLEN(100),XDIA(100),DELV(  GETREADY
     1100),SDELV(100),SUMDEL(100)                                         GETREADY
      DIMENSION XVOL(3,100)                                               GETREADY
      DIMENSION AZ(100,100)                                               GETREADY
      DATA SA(1),SA(2),SA(3)/10HVELOCITY (,10HMM/MICROSE,3HC)>/           GETREADY
      DATA SB(1),SB(2),SB(3)/10HCUMULATIVE,10H MASS (GRA,4HMS)>/          GETREADY
      DATA SC(1),SC(2),SC(3),SC(4)/10HPOSITION A,10HLONG JET L,1CHENGTH   GETREADY
     1(MM),1H>/                                                           GETREADY
      DATA SD(1),SD(2),SD(3)/10HCUMULATIVE,10H K.E. (JOU,5HLES)>/         GETREADY
      DATA SE(1),SE(2),SE(3),SE(4)/10HDISTANCE F,10HROM CHARGE,1CH BASE   GETREADY
     1(MM),1H>/                                                           GETREADY
      DATA SF(1),SF(2),SF(3)/10HBREAK-UP T,10HIME (MICRO,5HSEC)>/         GETREADY
      DATA SL1(1)/8HFLASH 1>/                                             GETREADY
      DATA SL2(1)/8HFLASH 2>/                                             GETREADY
      DATA SL3(1)/8HFLASH 3>/                                             GETREADY
      DATA MPA,MPAR,MPART,MCO,MCON,MCONT/4HPART,4HICUL,4HATED,4H CON,4HT  GETREADY
     1INU,4HOUS /                                                         GETREADY
    1 FORMAT(3I5,F5.2,6F10.5)                                             BRL2330
    2 FORMAT(7F10.5)                                                      BRL2330
    6 FORMAT(8F10.5)                                                      BRL2330
   21 FORMAT(2I5)                                                         BRL2330
   30 FORMAT(12I5,2X,I1,2X,3I5)                                           BRL2330
      READ(5,21) ICASES,LCL                                               BRL2330
      IF(EOF(5)) 23,23                                                    BRL2330
   23 DO 500 IJ=1,ICASES                                                  BRL2330
   22 READ(5,1)NROUND,NPART,NFLASH,RHC,(XMAG(I),I=1,3),FLASH1,FLASH2,     BRL2330
     1FLASH3                                                              BRL2330
      IF(EOF(5)) 24,24                                                    BRL2330
   24 ENCODE(21,20,ST(1)) NROUND                                          BRL2330
   20 FORMAT(10HROUND NUMB,4HER  ,I5,2H >)                                BRL2330
      READ(5,2) FOCUS1,FOCUS2,FOCUS3,F1A,F2A,F3A,F4A                      BRL2330
      IF(EOF(5)) 25,28                                                    BRL2330
   25 READ(5,6) F1B,F2B,F3B,F4B,F1C,F2C,F3C,F4C                           BRL2330
      IF(EOF(5)) 26,26                                                    BRL2330
   26 RO=RHO                                                              BRL2330
      IF(LCL.NE.1) GO TO 29                                               BRL2330
```

```
      RHO=0.                                                            BRL2330
C                                                                       BRL2330
C     ROUND INFORMATION CARD NEXT                                       BRL2330
   29 PRINT 5                                                           BRL2330
      PRINT 3, NROUND,RHO,(XMAG(N),N=1,3),FOCUS1,FOCUS2,FOCUS3,FLASH1,FL BRL2330
     1ASH2,FLASH3                                                       BRL2330
    3 FORMAT(/////,20X,'ROUND NUMBER    ',I5,//,20X,'LINER DENSITY(GM/CC)- BRL2330
     1 ',F4.1,/,20X,'MAGNIFICATION FACTOR-',3F9.5,/,20X,'DISTANCE FROM L BRL2330
     2INER BASE TO FOCAL POINT(MM)',/,25X,'FLASH 1- ',F6.1,/,25X,'FLASH BRL2330
     32- ',F6.1,/,25X,'FLASH 3- ',F6.1,/,20X,'DELAY TIMES (MICROSEC)',/, BRL2330
     425X,'FLASH 1- ',F6.1,/,25X,'FLASH 2- ',F6.1,/,25X,'FLASH 3- ',F6.1 BRL2330
     5)                                                                 BRL2330
      RHO=RO                                                            BRL2330
      PRINT 5                                                           BRL2330
    5 FORMAT(1H1)                                                       BRL2330
      PRINT 4                                                           BRL2330
    4 FORMAT(21X,'PARTICLE   AVG. VELOCITY    TOTAL JET      BREAK-UP',/,2 BRL2330
     12X,'NUMBER',4X,'(MM/MICROSEC)',3X,'LENGTH(MM)',3X,'(PICROSEC)',/) BRL2330
      PI=3.14159                                                        BRL2330
      DO 150 I=1,NFLASH                                                 BRL2330
      DO 149 J=1,NPART                                                  BRL2330
      READ(5,30)(IX(K),IY(K),K=1,6),L,IFILM,IROUND,IPART                BRL2330
      IF(EOF(5)) 32,32                                                  BRL2330
   32 DO 35 M=1,6                                                       BRL2330
      ZX(M)=FLOAT(IX(M))/15.5906                                        BRL2330
   35 ZY(M)=FLOAT(IY(M))/15.5906                                        BRL2330
      AZ(I,J)=((ZY(2)+ZY(5))/2.)*XMAG(I)                                BRL2330
      IF(ZX(1).EQ.ZX(2)) GO TO 40                                       BRL2330
      R1=.5*SQRT((ZX(1)-ZX(6))**2+(ZY(1)-ZY(6))**2)*XMAG(I)             BRL2330
      R2=.5*SQRT((ZX(2)-ZX(5))**2+(ZY(2)-ZY(5))**2)*XMAG(I)             BRL2330
      R3=.5*SQRT((ZX(3)-ZX(4))**2+(ZY(3)-ZY(4))**2)*XMAG(I)             BRL2330
      P1X=(ZX(1)+ZX(6))/2.                                              BRL2330
      P1Y=(ZY(1)+ZY(6))/2.                                              BRL2330
      P2X=(ZX(3)+ZX(4))/2.                                              BRL2330
      P2Y=(ZY(3)+ZY(4))/2.                                              BRL2330
      P3X=(ZX(2)+ZX(5))/2.                                              BRL2330
      P3Y=(ZY(2)+ZY(5))/2.                                              BRL2330
      XH1=SQRT((P1X-P3X)**2+(P1Y-P3Y)**2)*XMAG(I)                       BRL2330
      XH2=SQRT((P3X-P2X)**2+(P3Y-P2Y)**2)*XMAG(I)                       BRL2330
      P1Z=P1X                                                           BRL2330
      P1X=P2X                                                           BRL2330
      GOTO 45                                                           BRL2330
   40 P1X=ZX(1)                                                         BRL2330
   45 IF(L.EQ.2) GOTO 55                                                BRL2330
      IF(L.EQ.3) GOTO 65                                                BRL2330
      IF(IFILM.EQ.2) GO TO 47                                           BRL2330
      IF(IFILM.EQ.3) GO TO 48                                           BRL2330
      IF(IFILM.EQ.4) GO TO 49                                           BRL2330
      S1(J)=FOCUS1-(F1A-P1X)*XMAG(I)                                    BRL2330
      GO TO 15                                                          BRL2330
   47 S1(J)=FOCUS1-(F2A-P1X)*XMAG(I)                                    BRL2330
      GO TO 15                                                          BRL2330
   48 S1(J)=FOCUS1+(F3A+P1X)*XMAG(I)                                    BRL2330
      GO TO 15                                                          BRL2330
   49 S1(J)=FOCUS1+(F4A+P1X)*XMAG(I)                                    BRL2330
   15 IF(ZX(1).EQ.ZX(2)) GO TO 50                                       BRL2330
      L1(J)=0                                                           BRL2330
      GOTO 75                                                           BRL2330
   50 L1(J)=1                                                           BRL2330
      GOTO 80                                                           BRL2330
   55 IF(IFILM.EQ.2) GO TO 57                                           BRL2330
      IF(IFILM.EQ.3) GO TO 58                                           BRL2330
      IF(IFILM.EQ.4) GO TO 59                                           BRL2330
      S2(J)=FOCUS2-(F1B-P1X)*XMAG(I)                                    BRL2330
```

```
      GO TO 16
   57 S2(J)=FOCUS2-(F2B-P1X)*XMAG(I)
      GO TO 16
   58 S2(J)=FOCUS2+(F3B+P1X)*XMAG(I)
      GO TO 16
   59 S2(J)=FOCUS2+(F4B+P1X)*XMAG(I)
   16 V1(J)=(S2(J)-S1(J))/(FLASH2-FLASH1)
      IF(ZX(1).EQ.ZX(2)) GO TO 60
      L2(J)=0
      GOTO 75
   60 L2(J)=1
      GOTO 80
   65 IF(NFLASH.EQ.2) GOTO 80
      IF(IFILM.EQ.2) GO TO 67
      IF(IFILM.EQ.3) GO TO 68
      IF(IFILM.EQ.4) GO TO 69
      S3(J)=FOCUS3-(F1C-P1X)*XMAG(I)
      GO TO 17
   67 S3(J)=FOCUS3-(F2C-P1X)*XMAG(I)
      GO TO 17
   68 S3(J)=FOCUS3+(F3C+P1X)*XMAG(I)
      GO TO 17
   69 S3(J)=FOCUS3+(F4C+P1X)*XMAG(I)
   17 V2(J)=(S3(J)-S2(J))/(FLASH3-FLASH2)
      V3(J)=(S3(J)-S1(J))/(FLASH3-FLASH1)
      IF(ZX(1).EQ.ZX(2)) GO TO 70
      L3(J)=0
      GOTO 75
   70 L3(J)=1
      GOTO 80
   75 VOL(J)= VOL(J)+(PI*XH1/3.*(R1**2+R1*R2+R2**2)+PI*XH2/3.*(R2**2+R2*
     1R3+R3**2))
      P1X=P1Z
      XVOL(I,J)= PI*XH1/3.*(R1**2+R1*R2+R2**2)+PI*XH2/3.*(R2**2+R2*R3+
     1R3**2)
      XVOL(I,J)= XVOL(I,J)*.001*RHO
      XL(J)=XL(J)+SQRT((P1X-P2X)**2+(P1Y-P2Y)**2)*XMAG(I)
      DIA(J)=DIA(J)+2.*R2
   80 CONTINUE
      IF(I.LT.NFLASH) GOTO 149
      IF(NFLASH.EQ.2) GOTO 85
      IF(L1(J).EQ.1.AND.L2(J).EQ.1.AND.L3(J).EQ.1) GO TO 149
      IF(L1(J).EQ.0.AND.L2(J).EQ.0.AND.L3(J).EQ.0) GO TO 90
      IF(L2(J).EQ.1.AND.L3(J).EQ.1) GO TO 95
      IF(L1(J).EQ.1.AND.L3(J).EQ.1) GO TO 95
      IF(L1(J).EQ.1.AND.L2(J).EQ.1) GO TO 95
      IF(L2(J).EQ.0.AND.L3(J).EQ.0) GO TO 100
      IF(L1(J).EQ.0.AND.L3(J).EQ.0) GO TO 100
      IF(L1(J).EQ.0.AND.L2(J).EQ.0) GO TO 100
   85 IF(L1(J).EQ.1.AND.L2(J).EQ.1) GO TO 149
      IF(L1(J).EQ.0.AND.L2(J).EQ.0) GO TO 100
      IF(L1(J).EQ.0.OR.L2(J).EQ.0) GO TO 95
   90 XMASS(J)=VOL(J)*.001/3.*RHO
      XL(J)=XL(J)/3.
      DIA(J)=DIA(J)/3.
      GOTO 149
   95 XMASS(J)=VOL(J)*.001*RHO
      GOTO 149
  100 XMASS(J)=VOL(J)*.001/2.*RHO
      XL(J)=XL(J)/2.
      DIA(J)=DIA(J)/2.
  149 CONTINUE
  150 CONTINUE
C
```

```
C     BROK IS THE NUMBER OF JET PARTICLES THAT HAVE PARTICULATED AS OF
C     EXPOSURE TIMES 1, 2, AND 3 RESPECTIVELY.  TDLAY IS THE DELAY TIME
C     BETWEEN DETONATION AND JET FORMATION (MICROSEC).
C
      READ(5,*) BROK1,BROK2,BROK3,TDLAY
      PZ=BROK1+BROK2+BROK3
      TZ=FLASH1+FLASH2+FLASH3
      PBYTZ=BROK1*FLASH1+BROK2*FLASH2+BROK3*FLASH3
      PBYPZ=BROK1**2+BROK2**2+BROK3**2
      Z1=(PBYTZ-(PZ*TZ/3.))/(PBYPZ-(PZ**2/3.))
      PBAR=PZ/3.
      TAVG=TZ/3.
      DO 170 N=1,NPART
      IF(NFLASH.EQ.2)GOTO 155
      VEL(N)=(V1(N)+V2(N)+V3(N))/3.*.1
      GOTO 160
  155 VEL(N)=V1(N)*.1
  160 SUML(N)=XL(N)+SUML(N-1)
      SUMMAS(N)=XMASS(N)+SUMMAS(N-1)
      ELOD(N)=XL(N)/DIA(N)
      VEL(N)=VEL(N)*10.
      XKE(N)=.5*XMASS(N)*.001*(VEL(N)*1000.)**2
      SUMKE(N)=XKE(N)+SUMKE(N-1)
      P(N)=VEL(N)*XMASS(N)
      TOTP(N)=P(N)+TOTP(N-1)
      SUMDIA(N)=SUMDIA(N-1)+DIA(N)
      BREAK(N)=TAVG+Z1*(N-PBAR)-TDLAY
      GOTO 170
  165 BREAK(1)=0.0
  170 PRINT 171, N,VEL(N),SUML(N),BREAK(N)
  171 FORMAT(23X,I2,10X,F6.3,9X,F6.2,7X,F6.1)
      PRINT 52
   52 FORMAT(1H1,20X,'PARTICLE',4X,'VELOCITY1',6X,'VELOCITY2',6X,
     1'VELOCITY3',/,22X,'NUMBER',3X,'(MM/MICROSEC)',2X,'(MM/MICROSEC)',
     22X,'(MM/MICROSEC)',/)
      DO 172 J=1,NPART
  172 PRINT 173, J,V1(J),V2(J),V3(J)
  173 FORMAT(23X,I2,9X,F6.3,[illegible],F6.3,9X,F6.3)
      PRINT 175
  175 FORMAT(1H1,20X,'PARTICLE    LENGTH    DIA.    L/D     MASS      TOTAL J
     1ET',/,22X,'NUMBER',5X,'(MM)',4X,'(MM)',9X,'(GRAMS)',2X,'MASS(GRAMS
     2)',/)
      DO 176 I=1,NPART
  176 PRINT 177, I,XL(I),DIA(I),ELOD(I),XMASS(I),SUMMAS(I)
  177 FORMAT(23X,I2,8X,F4.1,4X,F4.3,2X,F4.1,4X,F5.2,5X,F6.2)
      PRINT 603
  603 FORMAT(1H1,20X,'PARTICLE',4X,'MASS1',9X,'MASS2',9X,'MASS3',/,22X,
     1'NUMBER',4X,'(GRAMS)',7X,'(GRAMS)',7X,'(GRAMS)',/)
      DO 600 J=1,NPART
      I=1
  600 WRITE(6,602) (J,XVOL(I,J),XVOL(I+1,J),XVOL(I+2,J))
  602 FORMAT(23X,I2,6X,F8.4,6X,F8.4,6X,F8.4)
      PRINT 180
  180 FORMAT(1H1,20X,'PARTICLE      K.E.      TOTAL JET    DISTANCE FROM CH
     1ARGE BASE',/,22X,'NUMBER',4X,'(JOULES)',3X,'KE(JOULES)',2X,'FLASH
     21',2X,'FLASH 2',2X,'FLASH 3',/)
      DO 181 I=1,NPART
  181 PRINT 182, I,XKE(I),SUMKE(I),S1(I),S2(I),S3(I)
  182 FORMAT(23X,I2,7X,F8.0,4X,F8.0,4X,F5.0,4X,F5.0,4X,F5.0)
      PRINT 183
  183 FORMAT(1H1,20X,'PARTICLE',4X,'MOMENTUM',4X,'TOTAL JET',/,22X,'NUMB
     1ER',4X,'(KG-M/SEC)',3X,'MOMENTUM',/)
      DO 185 I=1,NPART
  185 PRINT 184,I,P(I),TOTP(I)
```

```
  184 FORMAT(23X,I2,9X,F6.2,7X,F6.2)                                   BRL2330
      DO 192 N=2,NPART                                                 BRL2330
      SUMLEN(N)=SUMLEN(N-1)+XL(N)                                      BRL2330
      XDIA(N)=XDIA(N-1)+DIA(N)                                         BRL2330
      IF(N.EQ.2) GO TO 191                                             BRL2330
      DELV(N)=VEL(N-1)-VEL(N)                                          BRL2330
      GO TO 192                                                        BRL2330
  191 DELV(N)=VEL(1)-VEL(N)                                            BRL2330
  192 SDELV(N)=SDELV(N-1)+DELV(N)                                      BRL2330
      DO 195 J=3,NPART                                                 BRL2330
  195 SUMDEL(J)=DELV(J)+SUMDEL(J-1)                                    BRL2330
      AVL1=SUML(NPART)/FLOAT(NPART)                                    BRL2330
      AVL2=SUMLEN(NPART)/FLOAT(NPART-1)                                BRL2330
      AVD1=SUMDIA(NPART)/FLOAT(NPART)                                  BRL2330
      AVD2=XDIA(NPART)/FLOAT(NPART-1)                                  BRL2330
      ADELV1=SDELV(NPART)/FLOAT(NPART-1)                               BRL2330
      ADELV2=SUMDEL(NPART)/FLOAT(NPART-2)                              BRL2330
      PRINT 200, AVL1,AVL2,AVD1,AVD2,ADELV1,ADELV2                     BRL2330
  200 FORMAT(1H1,/////,47X,'WITH JET TIP     W/O TIP',/,20X,'AVERAGE PART BRL2330
     1ICLE LENGTH',7X,F6.2,7X,F6.2,/,20X,'AVERAGE PARTICLE DIAMETER',6X, BRL2330
     2F5.2,8X,F5.2,/,20X,'AVERAGE CHANGE IN VELOCITY',6X,F4.2,9X,F4.2)  BRL2330
      PRINT 505                                                        BRL2330
      NRA=2                                                            BRL2330
      NN=1                                                             BRL2330
      IC=0                                                             BRL2330
      CALL POLYLS(VEL,S1,NPART,AA,NRA,NN,CC,RR,AF,ERMS,SIG,TT,DET,IC)  BRL2330
      WRITE(6,41) CC(1)                                                BRL2330
      DS(1)=CC(1)                                                      BRL2330
   41 FORMAT(20X,' VIRTUAL ORIGIN FOR FLASH 1=',F12.6)                 BRL2330
      CALL POLYLS(VEL,S2,NPART,AA,NRA,NN,CC,RR,AF,ERMS,SIG,TT,DET,IC)  BRL2330
      WRITE(6,42) CC(1)                                                BRL2330
      DS(2)=CC(1)                                                      BRL2330
   42 FORMAT(20X,' VIRTUAL ORIGIN FOR FLASH 2=',F12.6)                 BRL2330
      IF(L.LT.3) GO TO 515                                             BRL2330
      CALL POLYLS(VEL,S3,NPART,AA,NRA,NN,CC,RR,AF,ERMS,SIG,TT,DET,IC)  BRL2330
      WRITE(6,43) CC(1)                                                BRL2330
      DS(3)=CC(1)                                                      BRL2330
   43 FORMAT(20X,' VIRTUAL ORIGIN FOR FLASH 3=',F12.6)                 BRL2330
C                                                                      DRIFT
C     DRIFT CALCULATIONS                                               DRIFT
C                                                                      DRIFT
C                                                                      DRIFT
C     EACH REF REFERS TO THE DISTANCE BETWEEN THE REFERENCE PARTICLE   DRIFT
C     AND THE FIDUCIAL FROM WHERE ALL OTHER MEASUREMENTS ARE TAKEN.    DRIFT
C     REF IS TAKEN IN MM AND SHOULD BE THE ACTUAL DISTANCE READ OFF OF DRIFT
C     THE FILM.  IT WILL THEN BE MULTIPLIED BY THE MAG FACTOR(WHICH    DRIFT
C     SHOULD HAVE BEEN ENTERED AS DATA IN BRL2330) NOTE, IF XMAG IS    DRIFT
C     LESS THAN 1. , THEN THE FILM PORTRAYS AN IMAGE LARGER THAN REALITY DRIFT
C                                                                      DRIFT
      READ(5,*) REF(1),REF(2),REF(3)                                   DRIFT
      REF(1)=REF(1)*XMAG(1)                                            DRIFT
      REF(2)=REF(2)*XMAG(2)                                            DRIFT
      REF(3)=REF(3)*XMAG(3)                                            DRIFT
      DO 401 J=1,3                                                     DRIFT
      DO 400 I=1,NPART                                                 DRIFT
  400 AZ(J,I)=AZ(J,I)-REF(J)                                           DRIFT
  401 CONTINUE                                                         DRIFT
      PRINT 33                                                         DRIFT
   33 FORMAT(1H1,21X,'PARTICLE',8X,'DEVIANCE FROM PATH (MM)',/,23X,    DRIFT
     1'NUMBER',6X,'FLASH 1     FLASH 2     FLASH 3',/)                 DRIFT
      DO 800 JJJ=1,NPART                                               DRIFT
      WRITE (6,36) JJJ,AZ(1,JJJ),AZ(2,JJJ),AZ(3,JJJ)                   DRIFT
   36 FORMAT(24X,I2,8X,F8.3,3X,F8.3,3X,F8.3)                           DRIFT
  800 CONTINUE                                                         DRIFT
```

```
      DO 491 I=1,NPART                                                  DRIFT
      T1(I)=(S1(I)-DS(1))/VEL(I)                                        DRIFT
      T2(I)=(S2(I)-DS(2))/VEL(I)                                        DRIFT
      T3(I)=(S3(I)-DS(3))/VEL(I)                                        DRIFT
      KD12=AZ(1,I)*T2(I)/(AZ(2,I)*T1(I))                                DRIFT
      KD23=AZ(2,I)*T3(I)/(AZ(3,I)*T2(I))                                DRIFT
      KD13=AZ(1,I)*T3(I)/(AZ(3,I)*T1(I))                                DRIFT
      DO 405 J=1,3                                                      DRIFT
      IF(AZ(J,I)+REF(J)) 405,402,405                                    DRIFT
  402 THETA(I)=0.0                                                      DRIFT
      VETRAV(I)=0.0                                                     DRIFT
      GO TO 491                                                         DRIFT
  405 CONTINUE                                                          DRIFT
C                                                                       DRIFT
C     SOLVING FOR THETA USING FIRST TWO GOVERNING EQUATIONS             DRIFT
C                                                                       DRIFT
      TH12=ATAN(2.0*KD12/SQRT(2.0)-1.0)                                 DRIFT
      IF(TH12.LT.0.0)TH12=TH12+PI                                       DRIFT
C                                                                       DRIFT
C     SOLVING FOR THETA USING LAST TWO GOVERNING EQUATIONS              DRIFT
C                                                                       DRIFT
      TH23=ATAN(1.0-2.0/(SQRT(2.0)*KD23))                               DRIFT
      IF(TH23.LT.0.0)TH23=TH23+PI                                       DRIFT
  450 IF(ABS(TH12-TH23).LT.PI/2.0)GO TO 449                             DRIFT
      IF(TH23.LT.TH12)GO TO 448                                         DRIFT
      TH12=TH12+PI                                                      DRIFT
      GO TO 449                                                         DRIFT
  448 TH12=TH12-PI                                                      DRIFT
C                                                                       DRIFT
C     SOLVING FOR THETA USING FIRST AND LAST GOVERNING EQUATIONS        DRIFT
C                                                                       DRIFT
  449 TH13=ATAN((KD13-1.0)/(KD13+1.0))                                  DRIFT
      IF(TH13.LT.0.0)TH13=TH13+PI                                       DRIFT
  470 IF(ABS(TH23-TH13).LT.PI/2.0)GO TO 469                             DRIFT
      IF(TH23.LT.TH13)GO TO 468                                         DRIFT
      TH13=TH13+PI                                                      DRIFT
      GO TO 469                                                         DRIFT
  468 TH13=TH13-PI                                                      DRIFT
C                                                                       DRIFT
C     FINDING AN AVERAGE VALUE FOR THETA AND PLACING IT IN THE PROPER   DRIFT
C     QUADRANT                                                          DRIFT
C                                                                       DRIFT
  469 THV=(TH12+TH23+TH13)/3.0                                          DRIFT
      IF((TH23-PI/2.0)*AZ(2,I)) 471,473,472                             DRIFT
  471 THETA(I)=THV                                                      DRIFT
      GO TO 480                                                         DRIFT
  472 THETA(I)=THV+PI                                                   DRIFT
      TH12=TH12+PI                                                      DRIFT
      TH23=TH23+PI                                                      DRIFT
      TH13=TH13+PI                                                      DRIFT
      IF(THETA(I)-THV.GT.1.7)THV=THV+PI                                 DRIFT
      GO TO 480                                                         DRIFT
  473 IF(TH13) 474,475,475                                              DRIFT
  474 THETA(I)=THV+PI                                                   DRIFT
      TH12=TH12+PI                                                      DRIFT
      TH23=TH23+PI                                                      DRIFT
       TH13=TH13+PI                                                     DRIFT
       IF(THETA(I)-THV.GT.1.7)THV=THV+PI                                DRIFT
      GO TO 480                                                         DRIFT
  475 THETA(I)=THV                                                      DRIFT
C                                                                       DRIFT
C     CALCULATING RELATIVE TRANSVERSE VELOCITIES WHILE ASSIGNING        DRIFT
C     WEIGHTED VALUES...(DEPENDING ON THE PARTICLES' ORIENTATION        DRIFT
C     WITH THE FLASH X-RAY)                                             DRIFT
```

```
C
  480 VETR12=AZ(1,I)/(COS(TH12-PI/4.0)*T1(I))*1000.0
      VETR23=AZ(2,I)/(COS(TH23)*T2(I))*1000.0
      VETR13=AZ(3,I)/(COS(TH13+PI/4.0)*T3(I))*1000.0
      EPS(1,I)=AZ(1,I)*SIN(TH12-PI/4.0)*(TH12-THV)/T1(I)*1000.0
     1          /(COS(TH12-PI/4.0))**2
      EPS(2,I)=AZ(2,I)*SIN(TH23)*(TH23-THV)*1000.0/T2(I)
     1          /(COS(TH23))**2
      EPS(3,I)=AZ(3,I)*SIN(TH13+PI/4.0)*(TH13-THV)/T3(I)*1000.0
     1          /(COS(TH13+PI/4.0))**2
      EPS(4,I)=AZ(1,I)*SIN(TH13-PI/4.0)*(TH13-THV)/T1(I)*1000.0
     1          /(COS(TH13-PI/4.0))**2
      EPS(5,I)=AZ(2,I)*SIN(TH12)*(TH12-THV)*1000.0/T2(I)
     1          /(COS(TH12))**2
      EPS(6,I)=AZ(3,I)*SIN(TH23+PI/4.0)*(TH23-THV)/T3(I)*1000.0
     1          /(COS(TH23+PI/4.0))**2
      DO 481 J=1,6
  481 EPS(J,I)=ABS(EPS(J,I))
      EPSUM=0.0
      DO 482 J=1,6
  482 EPSUM=1.0/EPS(J,I)+EPSUM
      DO 483 J=1,6
  483 WT(J)=1.0/(EPS(J,I)*EPSUM)
      VETRAV(I)=WT(1)*VETR12+WT(2)*VETR23+WT(3)*VETR13+WT(4)*VETR12
     1          +WT(5)*VETR23+WT(6)*VETR13
C
C     CONVFRT THETA TO DEGREES
C
  490 THETA(I)=180.0*THETA(I)/PI
  491 CONTINUE
      PRINT 492
  492 FORMAT(1H1,21X,'PARTICLE',5X,'RELATIVE TRANSVERSE',5X,'RELATIVE ',
     1       'DEVIANCE',/,23X,'NUMBER',8X,'VELOCITY (M/S)',9X,'ANGLE',
     2       ' (DEGREES)',/)
      DO 495 K=1,NPART
      WRITE(6,494) K,VETRAV(K),THETA(K)
  494 FORMAT(24X,I2,15X,F6.2,17X,F5.1)
  495 CONTINUE
C
C     TRANSLATE APPARENT VALUES INTO ABSOLUTE VALUES
C
      R(2)=0.0
C
C     GUESSING AT AN INITIAL DEVIANCE ANGLE FOR THE REFERENCE
C
      TMIN=THETA(1)
      TMAX=THETA(1)
      MINDEX=1
      MAXDEX=1
      DO 391 I=2,NPART
      IF(THETA(I).LT.TMIN.OR.TMIN-THETA(I).LT.-300.)GO TO 392
      GO TO 393
  392 TMIN=THETA(I)
      MINDEX=I
      GO TO 391
  393 IF(THETA(I).GT.TMAX.OR.TMAX-THETA(I).GT.300.) GO TO 394
      GO TO 391
  394 TMAX=THETA(I)
      MAXDEX=I
  391 CONTINUE
      IF(MINDEX.GT.MAXDEX) GO TO 395
      INCR=.0034907
      THETAO=THETA(MAXDEX)-180.
      GO TO 396
```

```
  395 INCR=-.0034907
      THETAD=THETA(MINDEX)-180.
  396 DRCS=0.0
      DO 899 I=1,NPART
      THETA(I)=THETA(I)*PI/180.0
      VX(I)=VETRAV(I)*COS(THETA(I))
  899 VY(I)=VETRAV(I)*SIN(THETA(I))
      THOR=THETAD*PI/180.0
  902 R(1)=R(2)
      ITOTL=IFIX(.122173/ABS(INCR))
      DO 1100 NOT=1,ITOTL
      THOR=THOR+INCR
  903 VTO=0.0
C
C     FINDING THE MAGNITUDE OF REFERENCE TRANSVERSE VELOCITYTHAT WILL
C     MAKE IT PROPORTIONAL TO THE AXIAL VELOCITY
C
      DO 756 I=1,NPART
  756 VTABS(I)=VETRAV(I)
  904 VTO=VTO+10.0
      INC=100
      GO TO 909
  905 VTO=VTO+1.0
      INC=10
      GO TO 909
  906 VTO=VTO+.1
      INC=1
  909 VXO=VTO*COS(THOR)
      VYO=VTO*SIN(THOR)
      DO 907 I=1,NPART
  907 VTABS(I)=SQRT((VX(I)-VXO)**2+(VY(I)-VYO)**2)
C
C     STATISTICAL CALCULATIONS FOR A LINEAR REGRESSION
C
  802 TS=0.0
      AS=0.0
      TBYAS=0.0
      TBYTS=0.0
      ABYAS=0.0
      KLESS=0
      DO 900 I=1,NPART
      IF(ABS(VTABS(I)-VTO) .LE. 1.0) GO TO 700
      TS=VTABS(I)+TS
      AS=VEL(I)+AS
      TBYAS=VTABS(I)*VEL(I)+TBYAS
      TBYTS=VTABS(I)**2+TBYTS
      ABYAS=VEL(I)**2+ABYAS
      GO TO 900
  700 KLESS=KLESS+1
  900 CONTINUE
      CO1=(TBYAS-(TS*AS/(NPART-KLESS)))/(TBYTS-(TS**2/(NPART-KLESS)))
      CO2=(TBYAS-(TS*AS/(NPART-KLESS)))/(ABYAS-(AS**2/(NPART-KLESS)))
      CO=(CO1+1.0/CO2)/2.0
      TBAR=TS/(NPART-KLESS)
      ABAR=AS/(NPART-KLESS)
      XINT=TBAR-ABAR/CO
      IF(XINT.LT.0.0 .AND. INC.EQ.100) GO TO 904
      IF(XINT.LT.0.0 .AND. INC.EQ.10) GO TO 905
      IF(XINT.LT.0.0 .AND. INC.EQ.1)  GO TO 906
      IF(INC-10) 912,911,910
  910 VTO=VTO-11.0
      GO TO 905
  911 VTO=VTO-1.1
      GO TO 906
```

```
  912 R(2)=SQRT(CO1*CO2)
      IF(R(2).GT.R(1)) GO TO 1101
      GO TO 1100
 1101 R(1)=R(2)
      VTOB=VTO
      THORB=THOR
      DO 1102 IB=1,NPART
 1102 VTB(IB)=VTABS(IB)
 1100 CONTINUE
      VTO=VTOB
      THOR=THORB
      DO 1103 IBI=1,NPART
 1103 VTABS(IBI)=VTB(IBI)
  798 DO 815 N=1,NPART
      IF((VTABS(N)-VTO).LE. 1.0) GO TO 811
      PHI(N)=THETA(N)-THOR
      BETA(N)=ASIN(VETRAV(N)*SIN(PHI(N))/VTABS(N))*180.0/PI
      AVST(N)=VEL(N)/VTABS(N)*1000.0
      GO TO 815
  811 VTABS(N)=0.0
      BETA(N)=0.0
      AVST(N)=0.0
  815 CONTINUE
      PRINT 702
  702 FORMAT(1H1,21X,'PARTICLE',5X,'ABSOLUTE TRANSVERSE',5X,'ABSOLUTE ',
     1         'ANGULAR',5X,'AXIAL VELOCITY OVER',/,23X,'NUMBER',9X,'VEL',
     2       'OCITY (M/S)',4X,'DEVIANCE WRT REFERENCE  TRANSVERSE VELOC',
     3         'ITY',/)
      DO 710 J=1,NPART
      WRITE(6,707) J,VTABS(J),BETA(J),AVST(J)
  707 FORMAT(24X,I2,16X,F6.2,15X,F6.1,17X,F6.2)
  710 CONTINUE
      PRINT 712,VTO
  712 FORMAT(/,22X,'THE TRANSVERSE VELOCITY OF THE REFERENCE IS ',
     1         F6.2,' M/S')
      PRINT 713, R(2)
  713 FORMAT(/,22X,'THE CORRELATION COEFFICIENT FOR THIS REGRESSION',
     1         ' IS ',F5.4)
C
C     * * * * * P E N J E T * * * * *
C
C
C     ECONST IS THE ENERGY REQUIRED TO CREATE ONE CUBIC-MM OF HOLE
C     VOLUME.  RHOJ IS JET DENSITY IN G/CU-MM. SIGJ IS JET STRENGTH IN
C     MEGAPASCALS..  RHOT AND SIGT ARE THE CORRESPONDING TARGET
C     VARIABLES
C
      READ(5,300)ECONST,RHOJ,SIGJ,RHOT,SIGT
  300 FORMAT(5F10.4)
C
C     ZMIN IS THE MINIMUM STANDOFF AT WHICH PENJET WILL EVALUATE THE
C     GIVEN DRIFT DISTRIBUTION.  ZMAX IS THE MAXIMUM STANDOFF TO BE
C     ANALYZED.  ZINC IS THE INCREMENT BETWEEN STANDOFF ANALYZATION.
C     ALL MEASUREMENTS ARE IN MM.
C
      READ(5,397)ZMIN,ZMAX,ZINC
  397 FORMAT(3F10.1)
      DO 301 I=1,NPART
      BETA(I)=BETA(I)*3.14159/180.
      RADIUS(I)=0.0
      PEN(I)=0.0
      RL(I)=XL(I)
      RVEL(I)=VEL(I)
  301 CONTINUE
```

```
      NM1=NPART-1
      GAMMA=SQRT(RHOT/RHOJ)
      ZSUBO=ZMIN-ZINC
      KZSUM=0
  250 ZSUBO=ZSUBO+ZINC
      KZSUM=KZSUM+1
      PENMAX(KZSUM)=0.
      ZSUB(KZSUM)=ZSUBO
C
C     THIS LOOP EVALUATES EACH DIGITIZED PARTICLE
C
  291 DO 209 I=1,NPART
      NCC(I)=0
      NQ=0
  269 T(I)=(ZSUBO-XL(I)-(DS(1)+DS(2)+DS(3))/3.-2.995)/VEL(I)
      DELT=3./VEL(I)
      JMIN=1
C
C     LOCATING A PARTICLE IN 3-D SPACE...THEN FINDING WHETHER IT STRIKES
C     THE HOLE PROFILE.  IF IT DOESN'T, THEN TIME IS INCREMENTED UNTIL
C     IMPACT OCCURS.
C
  201 T(I)=T(I)+DELT
  205 X(I)=VEL(I)/AVST(I)*T(I)*COS(BETA(I))
      Y(I)=X(I)*TAN(BETA(I))
      Z(I)=VEL(I)*T(I)-ZSUBO+XL(I)+(DS(1)+DS(2)+DS(3))/3.
      IF(NQ.EQ.2)  GO TO 210
      IF(Z(I).LT.0.0) GO TO 201
      IF(I.EQ.1 .AND. T(I).LT.BREAK(I))GOTO 202
      IF(I.EQ.1)GO TO 210
      KLESS=I-1
      DO 206 J=JMIN,KLESS
      IF(PEN(J).LT..01)GO TO 206
      V(I,1)=X(I)-X(J)
      V(I,2)=Y(I)-Y(J)
      V(I,3)=Z(I)-Z(J)
      VM(I)=SQRT(V(I,1)**2+V(I,2)**2+V(I,3)**2)
      VAM(I)=V(I,1)*GRAD(J,1)+V(I,2)*GRAD(J,2)+V(I,3)*GRAD(J,3)
      VAM(I)=ABS(VAM(I))
      VPM(I)=SQRT(ABS(VM(I)**2-VAM(I)**2))
      IF((VPM(I)+DIA(I)/2.)**2/RADIUS(J)**2+VAM(I)**2/PEN(J)**2.GT.1.0)
     1     GO TO 206
      IF(NQ.EQ.1)GO TO 210
      JMIN=J
      GO TO 201
  206 CONTINUE
  207 NQ=1
      IF(JMIN.EQ.KLESS .AND. Z(I).LE..1) GO TO 208
      T(I)=T(I)-DELT/6.0
      GO TO 205
  208 T(I)=(ZSUBO-XL(I)-(DS(1)+DS(2)+DS(3))/3.)/VEL(I)
      NQ=2
      GO TO 205
C
C     FINDING THE EFFECTS OF THE PARTICLE PENETRATION
C
  210 IF(I.NE.1 .AND. NQ.NE.2)GO TO 202
      GRAD(1,1)=0.0
      GRAD(1,2)=0.0
      GRAD(1,3)=1.0
      GO TO 251
C
C     IF A PARTICLE IS NOT IN THE CONTINUOUS MODE, THE AXIS OF
C     PENETRATION IS EVALUATED
```

```
C
  202 IF(T(I).LT.BREAK(I))NCC(I)=1
      IF(I.EQ.1 .AND. NCC(I).EQ.1)GOTO1999
      IF(T(I).LT.BREAK(I))XL(I)=XL(I)*T(I)/BREAK(I)
      IM1=I-1
      IF(T(I).LT.BREAK(I) .AND. Z(I).GT.Z(IM1))GOTO 1999
      DO 204 LJ=1,3
      VA(I,LJ)=GRAD(JMIN,LJ)*VAM(I)
      VP(I,LJ)=V(I,LJ)-VA(I,LJ)
      AR(I,LJ)=VA(I,LJ)/VAM(I)
  204 PR(I,LJ)=VP(I,LJ)/VPM(I)
      RGRAD(I,1)=VPM(I)*2./RADIUS(JMIN)**2
      RGRAD(I,2)=0.0
      RGRAD(I,3)=VAM(I)*2./PEN(JMIN)**2
      RGM(I)=SQRT(RGRAD(I,1)**2+RGRAD(I,3)**2)
      RGRAD(I,1)=RGRAD(I,1)/RGM(I)
      RGRAD(I,3)=RGRAD(I,3)/RGM(I)
      DO 214 LJ=1,3
  214 GRAD(I,LJ)=RGRAD(I,1)*PR(I,LJ)+RGRAD(I,3)*AR(I,LJ)
      GM=SQRT(GRAD(I,1)**2+GRAD(I,2)**2+GRAD(I,3)**2)
      DO 219 LJ=1,3
  219 GRAD(I,LJ)=GRAD(I,LJ)/GM
      GOTO 251
C
C     CONTINUOUS PENETRATION AXIS IS ALONG PARTICLE FLIGHT AXIS.
C
 1999 VECT=SQRT(X(I)**2+Y(I)**2+(Z(I)+ZSUBO-(DS(1)+DS(2)+DS(3))/3.)**2)
      GRAD(I,1)=X(I)/VECT
      GRAD(I,2)=Y(I)/VECT
      GRAD(I,3)=(Z(I)+ZSUBO-(DS(1)+DS(2)+DS(3))/3.)/VECT
  251 PENMAX(KZSUM)=XL(I)/GAMMA+PENMAX(KZSUM)
      IF(I.EQ.1 .OR. NQ.EQ.2 .OR. NCC(I).EQ.1)GOTO 262
C
C     EFFECTIVE LENGTH AND EFFECTIVE VELOCITY CALCULATIONS.
C
      XL(I)=GRAD(I,3)*XL(I)+SQRT(GRAD(I,1)**2+GRAD(I,2)**2)
     1      *DTA(I)
      VEL(I)=GRAD(I,3)*VEL(I)
C
C     PENETRATION CALCULATIONS AS A FUNCTION OF EFFECTIVE VELOCITY.
C
      IF(VEL(I).GT. .8) GO TO 260
      PEN(I)=0.0
      RADIUS(I)=0.0
      U(I)=0.0
      HVOL(I)=0.0
      GO TO 209
  260 IF(VEL(I).GT.1.4) GO TO 261
      U(I)=0.0
      HVOL(I)=XKE(I)/ECONST
      PEN(I)=(VEL(I)-.8)**2/.72*XL(I)
      RADIUS(I)=SQRT(3.*HVOL(I) /(2.*3.14159*PEN(I)))
      GO TO 209
  261 IF(VEL(I).GT.2.)GO TO 262
      U(I)=0.0
      HVOL(I)=XKE(I)/ECONST
      PEN(I)=(-(VEL(I)-2.)**2/.72+1.)*XL(I)
      RADIUS(I)=SQRT(3.*HVOL(I) /(2.*3.14159*PEN(I)))
      GO TO 209
  262 RAD=SQRT(VEL(I)**2*RHOJ*RHOT-2.*(RHOJ-RHOT)*(SIGJ-SIGT)/1.E6)
      U(I)=(RHOJ*VEL(I)-RAD)/(RHOJ-RHOT)
      PEN(I)=(RHOJ*VEL(I)*XL(I)-XL(I)*RAD)/(RAD-RHOT*VEL(I))
      HVOL(I)=XKE(I)/ECONST
      RADIUS(I)=SQRT(3.*HVOL(I) /(2.*3.14159*PEN(I)))
```

```
209 CONTINUE
279 WRITF(6,211)
211 FORMAT(1H1,10X,'PARTICLE',5X,'HOLE',6X,'IMPACT',3X,'PENETRATION ',
   1'PENETRATION',6X,'STATUS'//12X,'NUMBER',5X,'VOLUME',6X,'TIME',17X,
   2      'VELOCITY',/,23X,'(CU.MM)   (MICROSEC)',4X,'(MM)',5X,'(MM/',
   3        'MICROSEC)',/)
    DO 213 I=1,NPART
    IF(NCC(I).EQ.1)GOTO 281
    WRITE(6,212)I,HVOL(I),T(I),PEN(I),U(I),MPA,MPAR,MPART
    GO TO 213
281 WRITE(6,212)I,HVOL(I),T(I),PEN(I),U(I),MCO,MCON,MCONT
212 FORMAT(14X,I2,7X,F6.0,4X,F5.1,7X,F4.1,8X,F5.3,7X,3A4)
213 CONTINUE
    PMAX=0.0
    DO 215 I=1,NPART
    IF(Z(I).LE.PMAX) GO TO 215
    PMAX=Z(I)
    DPMAX=PEN(I)*GRAD(I,3)
215 CONTINUE
    PENSUM=PMAX+DPMAX
    PENT(KZSUM)=PENSUM
    WRITE(6,216)PENSUM
216 FORMAT(1HO,10X,'THE TOTAL PENETRATION PREDICTED BY THIS ',
   1      'PROGRAM IS ',F6.1,' MM')
    PRINT 257, ZSUBO
257 FORMAT(1HO,10X,'THESE VALUES WERE CALCULATED AT A  STANDOFF ',
   1           'OF ',F6.0,' MM.')
    WRITE(6,220)
220 FORMAT(1H1,14X,'X,Y, AND Z COORDINATES       PENETRATION  MAX CRA',
   1       'TER RADIUS  AXIAL DIRECTION OF PENETRATION')
    DO 218 I=1,NPART
    WRITE(6,217)I,X(I),Y(I),Z(I),PEN(I),RADIUS(I),GRAD(I,1),
   1        GRAD(I,2),GRAD(I,3)
217 FORMAT(11X,I2,5F10.2,3F10.4)
218 CONTINUE
    DO 263 I=1,NPART
    VEL(I)=RVEL(I)
    KWAL(I)=0
263 XL(I)=RL(I)
    IF(ZSUBO.LT.ZMAX) GO TO 250
    WRITE(6,290)
290 FORMAT(1H1,' VIRTUAL ORIGIN ZO(MM)      PENETRATION(MM)      MAX ',
   +      'PENETRATION(MM)',/)
    DO 289 I=1,KZSUM
289 WRITE(6,292)ZSUB(I),PENT(I),PENMAX(I)
292 FORMAT(10X,F5.0,T32,F7.2,T55,F7.2)
515 CONTINUE
505 FORMAT(1H1)
    DO 510 JN= 1,NPART
    VOL(JN)=0.
    XL(JN)=0.
510 DIA(JN)=0.
500 CONTINUE
    STOP
    END
```

"JETBREAK"

BREAK(N) - breakup time of particle N in μsec

BROK 1/2/3 - observed number of jet particles already particulated as of exposure 1/2/3

FLASH 1/2/3 - time after detonation of round for exposure of film 1/2/3

PBAR -
PBYPZ -
PBYTZ -
TAVG -
} statistical variables used in calculation of breakup time

TDLAY - time delay between detonation of round and formation of jet

Z1 - time between breakup of adjacent jet particles

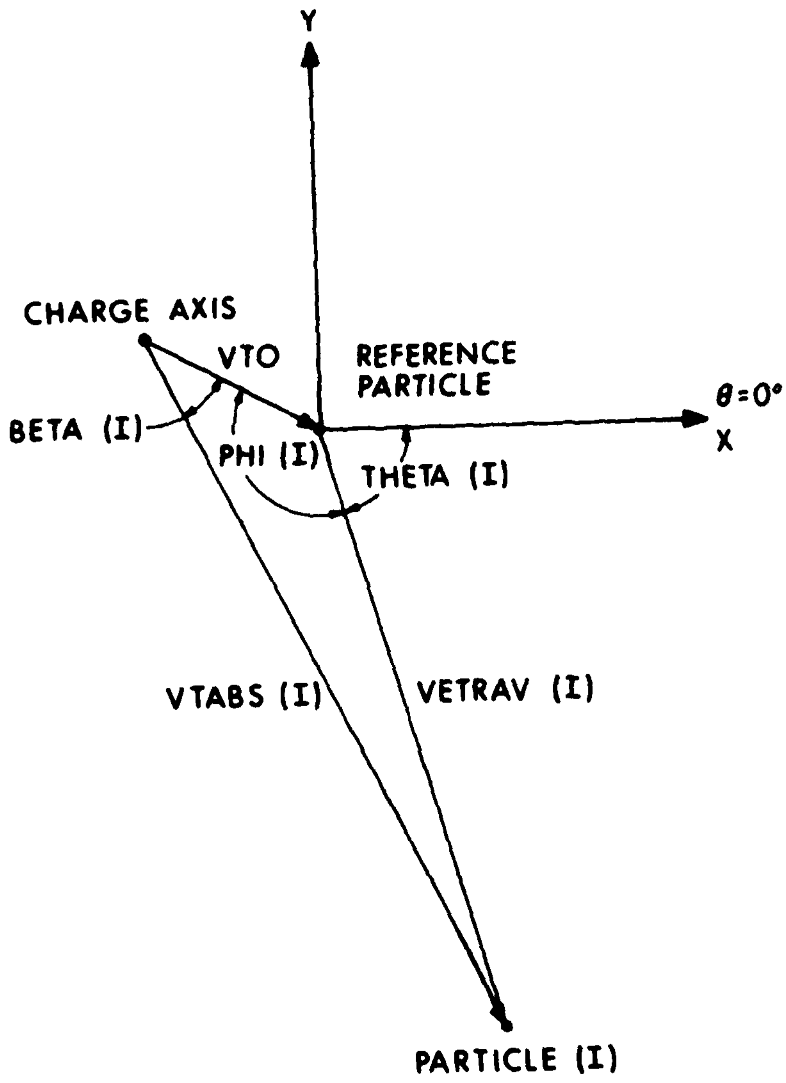

Figure A1. A Diagrammatic Sketch Identifying Some DRIFT Variables

"DRIFT"

AVST (I)	- the axial velocity divided by the transverse velocity for particle I
AZ (1, I) AZ (2, I) AZ (3, I)	- deviance of particle I with respect to the reference on exposure 1 2 3
BETA (I)	- absolute angle formed between drifting reference and particle I
DS (1) DS (2) DS (3)	- virtual origin calculations based on exposure 1 2 3
EPS (1, I) EPS (2, I) EPS (3, I) EPS (4, I) EPS (5, I)	- estimate for sensitivity of transverse velocity V with respect to small changes in drift angle Θ (of the form $\frac{dV}{d\Theta}\Delta\Theta$) using all combinations of drift velocities and drift angles calculated from the 3 radiographs
EPSUM	- $\sum_{K=1}^{6} \frac{1}{EPS(K, I)}$ a constant used to scale the EPS values to their proper magnitude
KD 12 KD 23 KD 13	- a constant relating time delay between exposures 1 and 2 2 and 3 1 and 3 used in drift velocity calculations
MAXDEX	- the particle # that satisfies TMAX
MINDEX	- the particle # that satisfies TMIN
PHI (I)	- the supplementary of the relative drift angle between particle I and the reference
R (2) R (1)	- correlation coefficient for V_A vs. V_T plot for reference drift angle presently being analyzed. previously
S1 (I) S2 (I) S3 (I)	- axial distance from charge base to particle I on exposure 1 2 3

T1 (I) }
T2 (I) } - estimated existence time from creation of particle I to exposure of film 1/2/3.
T3 (I) }

THETAO - initial guess at direction of reference drift

TMAX - the angle of the particle which is most clockwise/counterclockwise
TMIN in the relative angular span.

TH12 }
TH23 } - relative drift angle calculated from governing equations 1/2/1 and 2/3/3
TH13 }

THV - the numerical average of TH12, TH23, and TH13

THETA (I) - the relative drift angle of particle I with respect to arbitrary origin (chosen parallel to film 2) (degrees).

THOR - the current reference drift angle being tested

VETR12 }
VETR23 } - relative transverse velocity calculated from equations 1/2/1 and 2/3/3
VETR13 }

VETRAV (I) - relative transverse velocity of particle I based on weighted values of VETR12, VETR23, and VETR13 (m/s)

VTABS (I) - absolute transverse velocity of particle I (m/s)

VTO - transverse velocity of particle reference (m/s)

VXO - x component of drift velocity for the reference
VYO - y

VX (I) - x component of relative drift velocity for particle I
VY (I) - y

WT (I) - the percentage weight that an individual drift velocity calculation contributes to the overall average.

ABAR
ABYAS
AS
CO
CO1
CO2 } statistical variables used in V_A vs V_T regression
TBAR
TBYAS
TBYTS
TS
XINT

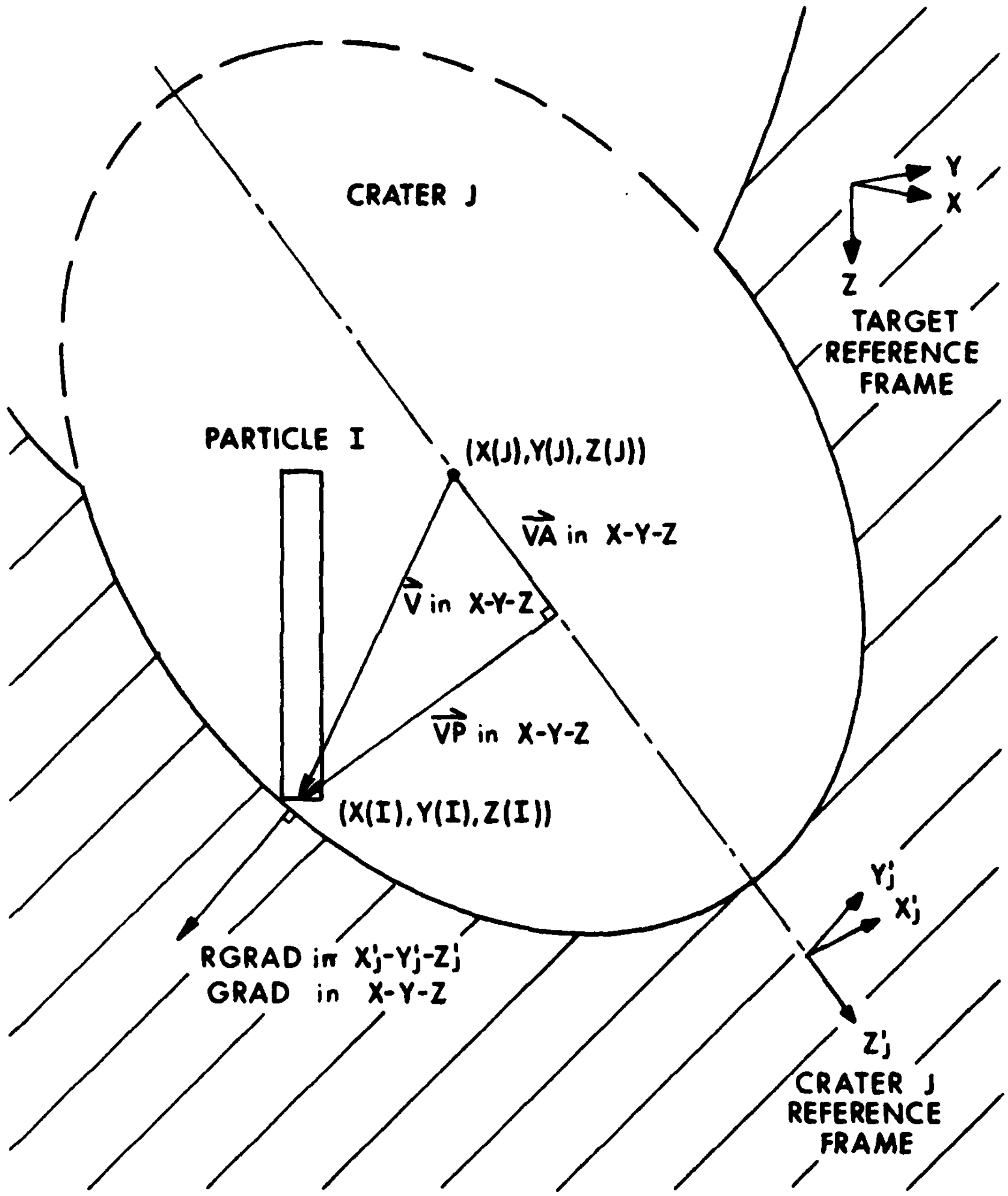

Figure A2: A Diagrammatic Sketch Identifying Some PENJET Variables.

"PENJET"

T (I) - impact time of particle I, taken from virtual origin

X (I), Y (I), Z (I) - spacial coordinates for top of particle I at any given time (and eventually upon impact) X = 0, Y = 0 denote where charge axis intersects target plate; Z = 0 is target surface.

DELT - time increment (varied so that particle travels 3 mm/timestep)

U (I) - penetration velocity of particle I (calculated only in the hypervelocity regime e.g. above 2 mm/μsec)

RADIUS (I) - crater radius of particle I

PEN (I) - penetration of particle I

HVOL (I) - hole volume created by particle I

V (I, 1), V (I, 2), V (I, 3) - the x, y, z components of a vector drawn from the center of crater J (through which particle I is instantaneously passing) to the tip of particle I

VM (I) - magnitude of vector $\vec{V}$

VA (I, 1), VA (I, 2), VA (I, 3) - the x, y, z components of vector $\vec{VA}$ which is in itself the component of vector $\vec{V}$ pointing axially down crater J (the crater through which particle I is passing)

VAM (I) - magnitude of vector $\vec{VA}$

VP (I, 1), VP (I, 2), VP (I, 3) - the x, y, z components of vector $\vec{VP}$ which is in itself the component of vector $\vec{V}$ pointing perpendicular to the penetration axis of crater J (through which particle I is passing). Note that $\vec{VA} + \vec{VP} = \vec{V}$

VPM (I) - magnitude of vector $\vec{VP}$

RGRAD (I, 1), RGRAD (I, 2), RGRAD (I, 3) - the x, y, z components of a vector that is perpendicular to crater J at the point of impact of particle I, but in the coordinate system of crater J (e.g., the Z' axis points down the axis of crater J)

RGM (I) - magnitude of vector $\overline{RGRAD}$

GRAD (I, 1)
GRAD (I, 2)
GRAD (I, 3) — the x, y, z components of a vector that is perpendicular to crater J at the point of impact of particle I, and in laboratory coordinate system (e.g., the axis points perpendicular to the target surface); $\overrightarrow{GRAD}$ becomes the axis of penetration for crater I according to refracted particle wave theory

GM (I) - magnitude of vector $\overrightarrow{GRAD}$

AR (I, 1)
AR (I, 2)
AR (I, 3) — a unit vector version of $\overrightarrow{VA}$

PR (I, 1)
PR (I, 2)
PR (I, 3) — a unit vector version of $\overrightarrow{VP}$

NCC (I) - equals 1 when particle I is particulate; equals 0 when I is continuous

ECONST - energy constant used for calculating crater volume (J/mm^3)

ZSUBO - standoff (mm) from virtual origin to target surface

RHOJ - jet density ρ_j (g/mm^3)

RHOT - target density ρ_t (g/mm^3)

SIGJ - jet strength (MPa)

SIGT - target strength (MPa)

GAMMA - $(\rho_t/\rho_j)^{1/2}$

JMIN - the last crater number that particle I has been known to successfully have passed through

PENSUM - the penetration resulting from PENJET calculations

NQ = 0 - particle I is travelling down hole profile

NQ = 1 - particle I has just struck target; t is decremented until precise impact time is revealed

NQ = 2 - particle I has drifted so far off course as to preclude entry into any part of the hole profile; it therefore strikes the target surface

KZSUM - number of standoffs at which PENJET has just analyzed a drift distribution

PENMAX (K) - the greatest possible penetration at standoff #K

ZSUB (K) - an array of the standoffs at which PENJET has just been run

PENT (K) - penetration predicted by PENJET at standoff #K

DISTRIBUTION LIST

No. of Copies	Organization
12	Commander Defense Technical Info Center ATTN: DTIC-DDA Cameron Station Alexandria, VA 22314
2	HQDA (DAMA-ZA; DAMA-RA, T. Rorstad) Washington, DC 20310
1	Assistant Secretary of the Army (R&D) ATTN: Assistant for Research Washington, DC 20310
1	Deputy Under Secretary of the Army (Operations Research) ATTN: SAUS-OR, D. C. Hardison Room 2E621, The Pentagon Washington, DC 20310
3	Commander US Army Materiel Development and Readiness Command ATTN: DRCDMD-ST DRCCG DRCDE-WM 5001 Eisenhower Avenue Alexandria, VA 22333
5	Commander US Army Armament Research and Development Command ATTN: DRDAR-TSS DRDAR-LCU-D-R/T. Stevens DRDAR-LCU-LT/A. King DRDAR-LCU-DC/J. Pearson Dover, NJ 07801
1	Commander US Army Armament Research and Development Command ATTN: DRDAR-TDC (Dr. D. Gyorog) Dover, NJ 07801
1	Commander US Army Armament Materiel Readiness Command ATTN: DRSAR-LEP-L Rock Island, IL 61299
1	Director US Army ARRADCOM Benet Weapons Laboratory ATTN: DRDAR-LCB-TL Watervliet, NY 12189
1	Commander US Army Aviation Research and Development Command ATTN: DRDAV-E 4300 Goodfellow Blvd St. Louis, MO 63120
1	Director US Army Air Mobility Research and Development Laboratory Ames Research Center Moffett Field, CA 94035
1	Commander US Army Communications Research and Development Command ATTN: DRSEL-ATDD Fort Monmouth, NJ 07703
1	Commander US Army Electronics Research and Development Command Technical Support Activity ATTN: DELSD-L Fort Monmouth, NJ 07703
9	Commander US Army Missile Command ATTN: DRSMI-R DRSMI-J COL C. M. Matthews, Jr. DRSMI-VIT DRCPM-HD/COL Cass DRCPM-HDE-M/R. Masucci DRCPM-TO DRSMI-YDL TOW-PM/COL Williamson DRSMI-RLA/E. B. Harwell Redstone Arsenal, AL 35898
2	Commandant US Army Infantry School ATTN: ATSH-CD-CSO-OR Fort Benning, GA 31905

DISTRIBUTION LIST

No. of Copies	Organization
3	Commander US Army Tank Automotive Command ATTN: DRDTA-RWL/C. Bradley DRDTA-TSL DRDTA-RC/Dr. J. Jellinek Warren, MI 48090
1	Program Manager XM1 Abrams Tank System ATTN: DRCPM-GCM-S Warren, MI 48090
1	Director US Army TRADOC Systems Analysis Activity ATTN: ATAA-SL White Sands Missile Range NM 88002
2	Commander US Army Materials and Mechanics Research Center ATTN: DRXMR-PDD/J. Prifti Tech Lib Watertown, MA 02172
1	Commander US Army Research Office P. O. Box 12211 Research Triangle Park NC 27709
2	Chief of Naval Research Department of the Navy ATTN: Code 427 Code 470 Washington, DC 20360
1	Commander Naval Sea Systems Command Washington, DC 20360
2	Commander Naval Air Systems Command ATTN: Code AIR-310 Code AIR-350 Washington, DC 20360
2	Commander Naval Surface Weapons Center ATTN: Code DG-50 DX-21, Lib Br Dahlgren, VA 22448 22448
1	Commander Naval Surface Weapons Center ATTN: Code 730, Lib Silver Spring, MD 20910
1	Commander Naval Surface Weapons Center ATTN: N. Coleburn Silver Spring, MD 20910
1	Commander Naval Weapons Center ATTN: Dr. L. Smith China Lake, CA 93555
2	Commander Naval Weapons Center ATTN: Code 4057 Code 3431, Tech Lib China Lake, CA 93555
1	Commander Naval Research Laboratory Washington, DC 20375
1	USAF/AFRDDA Washington, DC 20311
1	AFSC/SDZ/SDOA Andrews AFB Washington, DC 20334
2	US Air Force Academy ATTN: Code FJS-41 (NC) Tech Lib Colorado Springs, CO 80840
1	AFATL/DLJW (Dr. J. Foster) Eglin AFB, FL 32542
1	AFWL/SUL Kirtland AFB, NM 87117

DISTRIBUTION LIST

No. of Copies	Organization
1	AFATL/DLYV (Mr. J. Smith) Eglin AFB, FL 32542
1	AFWL/SUL (LT Tennant) Kirtland AFB, NM 87117
1	AFAL Wright-Patterson AFB, OH 45433
1	AFLC/MMWMC Wright-Patterson AFB, OH 45433
1	Director Lawrence Livermore National Lab. ATTN: Tech Lib P. O. Box 808 Livermore, CA 94550
2	Director Lawrence Livermore National Lab. ATTN: Dr. C. Godfrey Mr. M. Wilkins P. O. Box 808 Livermore, CA 94550
1	AFELM, The Rand Corporation ATTN: Library D 1700 Main Street Santa Monica, CA 90406
1	Sandia Laboratories ATTN: Tech Lib Albuquerque, NM 87115
1	Battelle- Memorial Institute ATTN: Mr. Joseph E. Backofen 505 King Avenue Columbus, OH 43201
1	Dyna East Corporation ATTN: P. C. Chou 227 Hemlock Road Wynnewood, Pa 19096
2	Firestone Defense Research and Products Division of the Firestone Tire and Rubber Company ATTN: R. Berus, L. Swabley 1200 Firestone Parkway Akron, OH 44317
1	Honeywell Inc. Government and Aerospace Products Division ATTN: C. R. Hargreaves 600 Second Street Hopkins, NM 55343
1	Physics International ATTN: Ron E. Brown San Leandro, CA 94577
1	Drexel Institute of Technology 32nd and Chestnut Streets Philadelphia, PA 19104
1	Systems, Science & Software ATTN; Dr. R. Sedgwick P. O. Box 1620 La Jolla, CA 92037

Aberdeen Proving Ground

Dir, USAMSAA
ATTN: DRXSY-D
DRXSY-MP, H. Cohen
DRXSY-G, Mr. Kramer
Cdr, USATECOM
ATTN: DRSTE-TO-E
Dir, USACSL, Bldg. E3516, EA
ATTN: DRDAR-CLB-PA
DRDAR-CLN
DRDAR-CLJ-L

USER EVALUATION OF REPORT

Please take a few minutes to answer the questions below; tear out this sheet, fold as indicated, staple or tape closed, and place in the mail. Your comments will provide us with information for improving future reports.

1. BRL Report Number ______________________________

2. Does this report satisfy a need? (Comment on purpose, related project, or other area of interest for which report will be used.)

____

____

____

3. How, specifically, is the report being used? (Information source, design data or procedure, management procedure, source of ideas, etc.) ______________________________

____

____

4. Has the information in this report led to any quantitative savings as far as man-hours/contract dollars saved, operating costs avoided, efficiencies achieved, etc.? If so, please elaborate.

____

____

5. General Comments (Indicate what you think should be changed to make this report and future reports of this type more responsive to your needs, more usable, improve readability, etc.) __________

____

____

____

6. If you would like to be contacted by the personnel who prepared this report to raise specific questions or discuss the topic, please fill in the following information.

Name: ______________________________

Telephone Number: ______________________________

Organization Address: ______________________________

____

____

— — — — — — — — — — FOLD HERE — — — — — — — — — —

Director
US Army Ballistic Research Laboratory
ATTN: DRDAR-BLA-S
Aberdeen Proving Ground, MD 21005

NO POSTAGE NECESSARY IF MAILED IN THE UNITED STATES

OFFICIAL BUSINESS
PENALTY FOR PRIVATE USE, $300

BUSINESS REPLY MAIL
FIRST CLASS PERMIT NO 12062 WASHINGTON, DC

POSTAGE WILL BE PAID BY DEPARTMENT OF THE ARMY

Director
US Army Ballistic Research Laboratory
ATTN: DRDAR-BLA-S
Aberdeen Proving Ground, MD 21005

— — — — — — — — — FOLD HERE — — — — — — — — —